

Shock & Vibration Isolation for an Electric Jet Ski

Alexander Dale Morgan

21396514

Master of Professional Engineering
School of Mechanical Engineering

Supervisor: Prof. Thomas Bräunl
School of Electrical, Electronic and Computer Engineering

University of Western Australia
Semester 1 of 2018

Word Count of Body: 7975



Alexander Morgan
130 Winthrop Ave
Crawley WA 6009

28th June 2018

Winthrop Professor John Dell
Executive Dean
Faculty of Engineering and Mathematical Sciences
The University of Western Australia
35 Stirling Highway
Crawley WA 6009

Dear Professor Dell,

I am pleased to submit this Master's thesis, entitled *Shock & Vibration Isolation for an Electric Jet Ski*, as part of the requirements for the degree of Master of Professional Engineering.

Yours sincerely,

Alexander Morgan

21396514

Acknowledgements

I would firstly like to thank my friends, Chris and Xu, for their continued support, suggestions, and empathy throughout this year-long challenging thesis project. I would also like to thank my peers for keeping my morale up with quality banter, and especially Jacob for his help in troubleshooting the Arduino. In addition, I want to thank my girlfriend Praise, and my parents for their emotional support.

I also want to thank my supervisor, Prof. Thomas Bräunl for holding me accountable to my actions and making me strive to perform at my best. From his teachings, I learned more about another discipline. Moreover, I would like to thank Ivan Neubronner for sharing his expertise in electrical engineering and troubleshooting.

I want to thank my mentor, Marcus Pham for his guidance on Arduino coding, and the Jet Ski in general. I also want to extend my deepest gratitude to Andrew Youssef for sharing his knowledge in vibrations and shocks. Andrew acted as the sole mentor that could guide me in my area of study where others could not.

Lastly, I want to thank my hardworking teammates, Maximillian and Patrick, for the countless hours they had put into this project and supporting one another.

Table of Contents

Acknowledgements.....	2
Nomenclature.....	5
Glossary of Terms.....	5
Project Summary.....	6
Introduction.....	7
Renewable Energy Vehicle.....	7
Recent Modifications.....	7
Project Scope.....	10
Problem Identification.....	10
Project Objectives.....	12
Design Criteria.....	12
Constraints.....	13
Literature Review.....	14
PWC Mounting Systems.....	14
Vibration Isolation.....	15
Design Process.....	17
Data Collection.....	17
Accelerometer.....	17
Recording Process.....	18
Field Data Processing.....	18
Design Options.....	22
Active & Passive Isolation Systems.....	22
Passive Isolation Options.....	23
Design Option Selection.....	26
Mount Design.....	28
Material Selection.....	30
Testing Frame.....	31
Testing Procedure.....	32
Data Processing.....	34
Results & Discussion.....	35
MC and Plate Mass System.....	36
Three Axes Average Maximum Response.....	36
Three Axes Fast Fourier Transform.....	38
Set Selection.....	40

Lighter Component Mass System	40
Three Axes Average Maximum Response	40
Three Axes Fast Fourier Transform	42
Set Selection	43
Comments on the Y-Axis	43
Installation of Mounting System	44
Conclusion	52
Future Work	53
References	55
Appendices.....	57
Appendix 1: Arduino Uno Accelerometer Code.....	57
Appendix 2: MATLAB Fourier Transform Code	61
MATLAB Code Usage	61
Plotting the Results	65
Appendix 3: Additional Benefits.....	66
Tube Loading.....	66
Centre of Mass.....	67
Appendix 4: Additional Research	68
Sampling Frequency	68
Fourier Transform.....	68

Nomenclature

Acronym	Description
DC-DC converter	Direct Current to Direct Current Converter
MC	Motor Controller
PWC	Personal Watercraft
REV Ski	Renewable Energy Vehicle Jet Ski
UWA	University of Western Australia

Glossary of Terms

Term	Definition
DC-DC converter	A device which serves to adjust voltage.
Fuses	Thin wires designed to melt when the current amperage is too great.
Motor Controller	A device which toggles the rotational velocity of the motor.

Project Summary

Electrical components within a vehicle are designed to fulfil their immediate function and at times, do not account for other aspects such as mechanical shocks or vibrations. Consequently, an additional system needs to be introduced for the purposes of either damping or reducing the vibrations and shocks experienced by the components. The goal of this system is to reduce the transmission of energy and the associated forces experienced by the components. This is for their protection and also to increase the longevity of each component. This is of particular importance for fuses, as mechanical shocks could lead to their failure. In turn, fuses would require frequent replacement which is not ideal in the context of transportation.

The Renewable Energy Vehicle PWC (REV Ski) experiences this very situation with its main electrical components. Those that require shock and vibration protection consist of fuse boxes, a DC-DC converter, a MC, and others. These components were bolted to aluminium plates, which were screwed into laminated wood adhered to the REV Ski hull.

To effectively design this system, field data was collected through the use of an accelerometer and Arduino Uno. This setup analysed the forces exerted on the MC box, and recorded them to a memory card. Through data processing, the forces and displacements of the system were obtained. This allowed for the appropriate selection of rubber mounts, which were subjected to additional tests to gather empirical knowledge on their performance, and thus suitability as a shock absorber.

Future works could involve the researching of active isolation. Should the benefits of which outweigh the disadvantages (monetary costs and power draw from the batteries), students could design a system of sensors and actuators to better isolate the components from shocks and vibrations.

Introduction

Recently, individuals have become more aware of their actions and its impacts on the planet. Since the industrial revolution, emission rates have soared, contributing greatly to climate change (Jones 2017). An increasing population has two severe effects on the environment. Namely, the augmented usage of fossil fuels, and a larger demand for animal farming, which is also a significant contributor to climate change (ClimateNexus 2018).

Societies are therefore seeking suitable alternatives to reduce fossil fuel emissions. Options such as nuclear power, natural gas, and renewable energy are being explored, each with its benefits and disadvantages. For renewable energy, its main advantage is that the source of energy cannot be depleted. On the other hand, the performance (power generation...etc), typically pales in comparison to traditional methods. Moreover, renewables are often associated with high capital costs, however, it is an area that is being researched and developed in order to render this technology economically viable. The movement to a dependence on renewables has already begun (Hunt 2017).

Renewable Energy Vehicle

At UWA, the REV Ski, is a renewable vehicle that is currently under development. It is a student project under the supervision of Professor Bräunl that began in 2012. The goal is to produce a safe and quieter, zero-emission PWC. It must also be comparable in terms of its performance and ride experience to that of the traditional PWCs. As a renewable vehicle, its source of power is through solar charging. In turn, this would be a sustainable product that addresses the concerns of the public, with the added benefit of significantly less noise pollution.

The conversion of a 2008 Sea-Doo 4-TEC model has resulted in several changes on the interior components of the PWC. As it is in the prototype phase, students are still discovering aspects of the vehicle that require addressing.

Recent Modifications

After test rides in 2015, users commented on the nose heavy tendency of the PWC. The bow was too close to the water, resulting in an uncomfortable ride position, and inefficiencies in the ride performance (Liu 2017).

In 2017 there had been a significant adjustment to its weight distribution. Battery tubes, the heaviest component in the PWC, were once situated from its centre to the front, and were repositioned to the centre-rear. This shifted the centre of mass of the vehicle towards further back, see Figure 1, thus improving the ride performance and user experience.

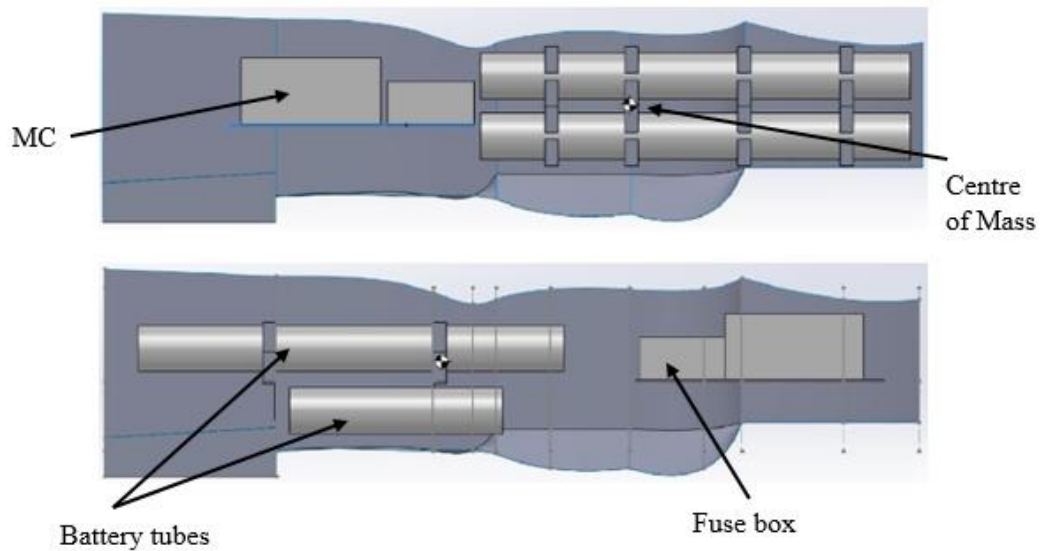


Figure 1: A cross-section view of the PWC interior from the starboard side. The top image is prior to 2017, with the tubes located at the centre-front of the PWC. Post 2017, these were repositioned to the centre-rear as displayed in the bottom image.

Prior to 2017, battery tubes were clamped in place by laminated wooden cradles (Figure 2), and the MC box and fuse box were mounted on top of the motor (Figure 3).

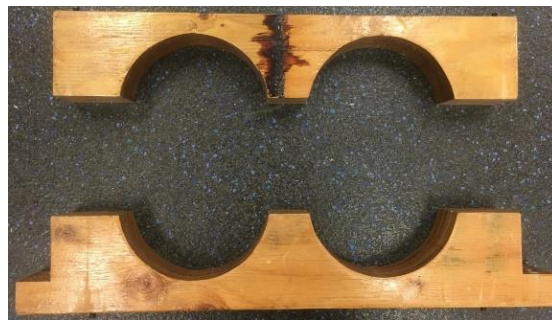


Figure 2: Wooden laminated cradles for battery tubes.

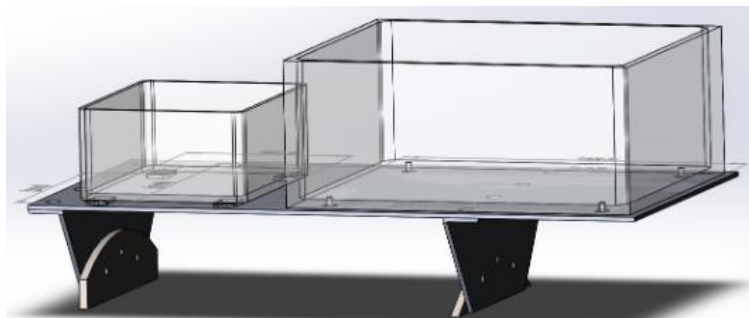


Figure 3: Previous mount for fuse box (left) and MC box (right), situated on the motor (Jensen 2015).

Now, the tubes are secured by a new battery mounting system, see Figure 4.



Figure 4: Partially disassembled battery mount reveals small battery tube (top), and two large tubes.

Due to the repositioning of the tubes, these components had to be relocated to the front of the PWC, as shown in Figure 1 and 5.



Figure 5: Relocated position of the MC box and other components at the bow.

Project Scope

Problem Identification

The laminated wooden cradles were adhered to the interior of the PWC hull. As a temporary solution after the repositioning of the tubes, the MC box and other components were fastened onto these cradles due to time constraints. Components were bolted onto aluminium plates, and these plates were screwed into the cradles, see Figures 6 and 7.



Figure 6: MC box and components are bolted to plates.

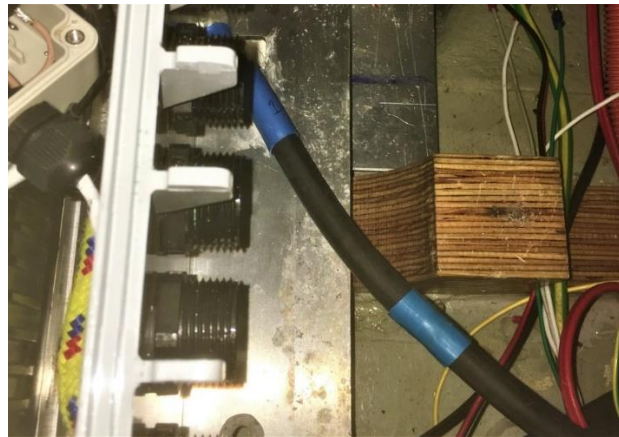


Figure 7: The small plate on the right in Figure 6 was removed, revealing how it was screwed into the laminated wooden cradles.

However, given the orientation of the laminated sheets on the cradles, the screws were entering between layers of wood, see Figure 8.



Figure 8: The screw on the right enters between the laminated sheets of wood.

Thus, the screw that is held in place does not employ the strength of the wood. Instead, the screws are only secured by the glue between the layers of wood. Hence, should a sufficient force be applied to the PWC from beneath (i.e. high impact force from waves), the screws may strip out of the cradles. This could lead to equipment damage and possible injury to the rider.

Often, electrical components serve to fulfil their function and do not account for shock or vibrations. This aspect may not be considered in their design criteria as the component is not supposed to be subjected to physical abuse, such as fuses for example. Given the context of an electric PWC, it has more electrical components to protect with fuses than the traditional. Therefore, it is more critical that fuses are protected. It would be inappropriate for fuses to fail due to shocks or vibrations from waves when the user is far from shore. This also applies to other components such as the DC-DC converter, and the data collection box which contains sensitive instrumentation. Therefore, by reducing the shocks transmitted from the waves to the components, it will protect them and prolong their longevity. The benefits associated with this is a reduction in the future costs of component replacement. Also, less labour hours will be dedicated to repairs and maintenance, and more on furthering the PWC.

Yet, the MC is designed to account for shocks and vibrations. It operates through switches, which are controlled by voltage and coils (Curtis Instruments 2009). Should a sufficient shock be applied, it may force a switch to flip. In turn, the PWC could alter its behaviour without the command of the user resulting in the rider potentially losing control. Although the likelihood of this occurring is low, it would be substandard engineering practice to default on one failsafe. Should shocks and vibrations be reduced prior to reaching the MC, it will further improve the safety and reliability of the PWC.

Project Objectives

The goal of this project is to design, construct, and install a mounting system to protect electronic components such as the MC box, fuse box, and other components. The focus of this design is to reduce the transmission of shocks and vibrations caused by waves and road features (during transportation), to the components.

Design Criteria

As established, the design of the mounting system must account for shocks and vibrations. In addition, the operating environment must also be considered. This is with regards to corrosion prevention, and waterproofing. Further, the mounting system must be user friendly.

As evident in Figure 1 and 9, the MC box is closer to the bow. Given this setup, the user operates blindly when conducting tasks on the fuse box. This is because the side of the MC box blocks a direct line of sight to the fuse box. As such, this reduces the user to working by touch and significantly increases the amount of time that is spent on mundane tasks. Given the nature of fuses, the user will need to access the fuse box more often than the MC box. Thus, the fuse box should be in an easily accessible location.

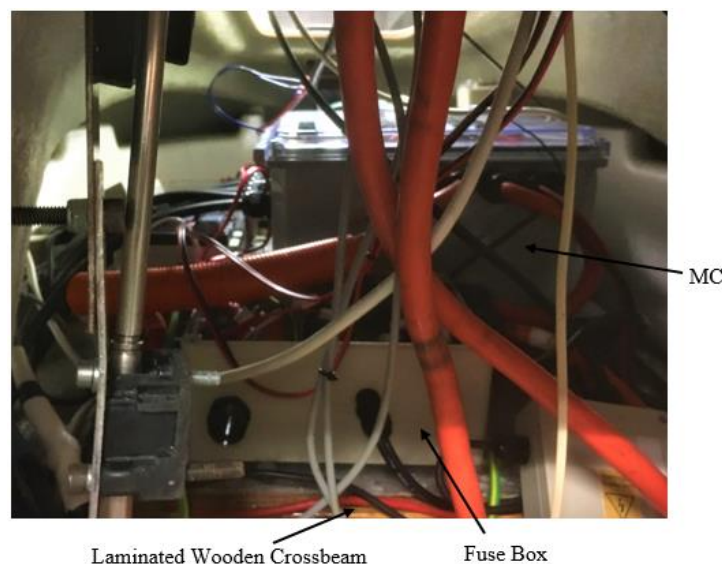


Figure 9: The view of the MC and fuse box from the rear of the PWC.

Furthermore, the mounting system should allow for the user to customize the positioning of components, with relative ease for the sake of future students. Previously, components were bolted to the plate, which was screwed into the laminated wood. However, given that some bolts were inaccessible, at times only three bolts were secured instead of four which was not ideal. It should also be noted that the positioning of the MC box directly under the opening reduces the ease of accessing other components such as the blade fuse box. As a result, maintenance and troubleshooting tasks on other components will require more time.

The mount should be as light as possible to reduce the overall mass of the PWC. Significant mass will result in a PWC that rides deeper through the water, which will reduce its ride performance due to greater drag forces. This will reduce its velocity and ride time.

Constraints

The mounting design was limited to constraints:

- The budget allocated to this project was \$500.
- To maintain the integrity of the hull, students were forbidden from drilling holes into the fibreglass.
- The interior of the PWC bow was space restricted, meaning that the surface area available for mounting components, and the height from this surface must be considered. When considering space efficiency, this includes the volume of components, its connecting wires, and the space needed by the user to install or extract components.

Literature Review

PWC Mounting Systems

The REV Ski team had developed various mount designs. Clark (2013) designed a mounting system for the MC, situated on top of the motor, see Figure 10.

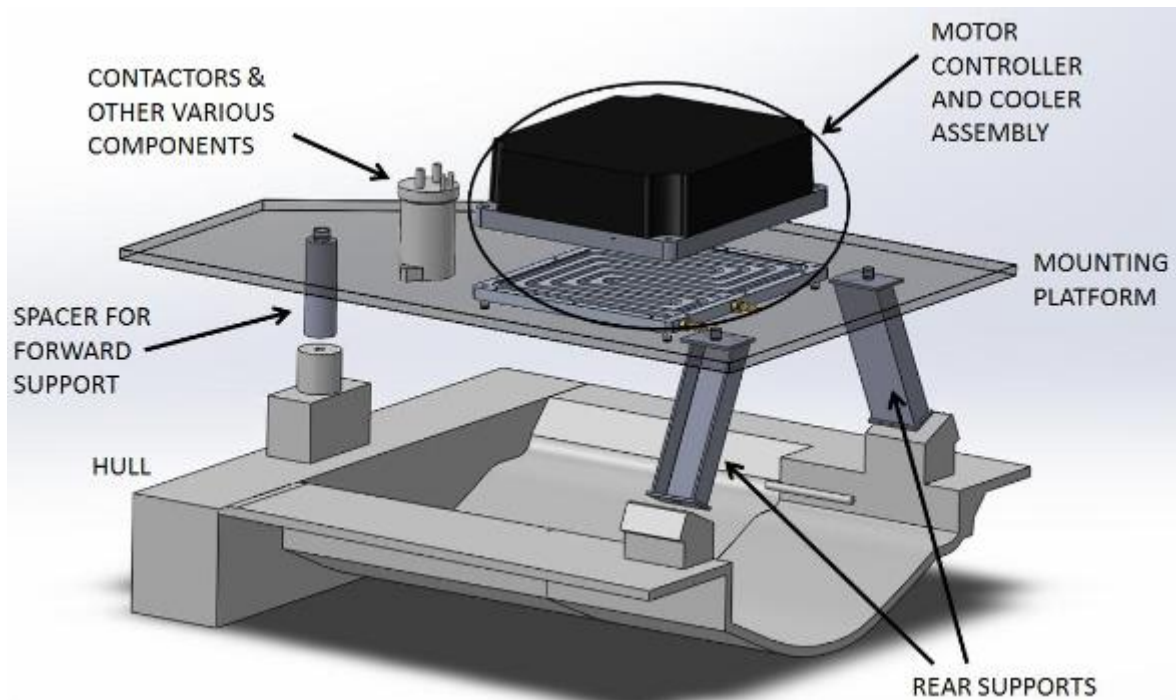


Figure 10: Clark's design for mounting the MC above the motor (Clark 2013).

This design employs fasteners which depend on the original mounting points from the combustion engine.

Jensen (2015) revised this mount and installed a system which held the MC and fuse box. This utilised fasteners, which passed through the holes in Figure 11, securing it to the motor.

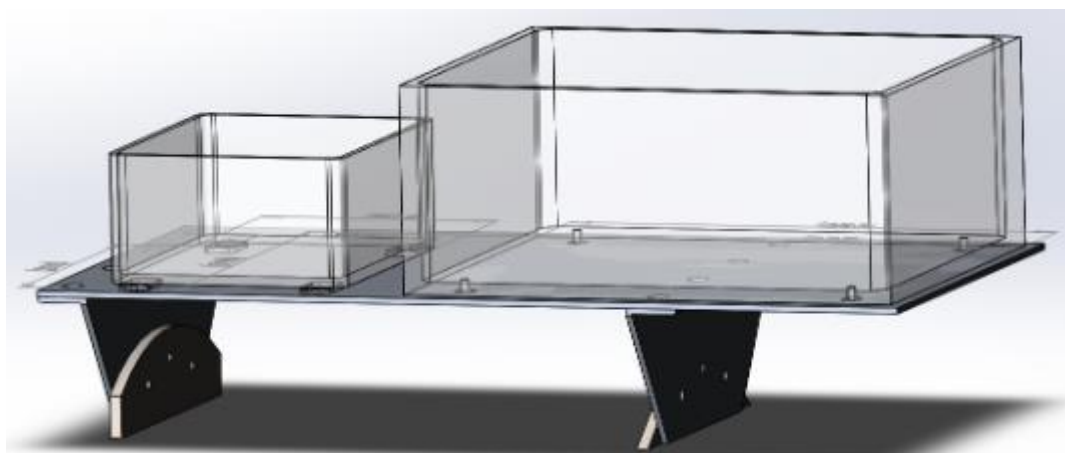


Figure 11: The most recent mounting system for the MC and fuse box prior to this project (Jensen 2015).

Similarly, Chau (2017) installed a battery mount (Figure 12) which depended on the motor and original mounting points for securing itself.



Figure 12: The latest battery mounting system (Chau 2017).

Vibration Isolation

The natural frequency of a system (*rad/s*) is the frequency at which it oscillates freely after an initial disturbance (Harris 2002). It has the following relationship:

$$\text{Natural Frequency} = \sqrt{\frac{\text{Spring Stiffness of System}}{\text{Mass of System}}}$$

The driving force is associated with the frequency at which the force is exerted, the excitation frequency. If the excitation frequency and the natural frequency coincide, the vibration amplitudes will increase. This is resonance (Harris 2002). Larger amplitudes could lead to catastrophic failure of equipment and injuries.

Vibrations and shocks may be reduced by:

- reducing the vibrations at the source by balancing moving masses (Harris 2002).
- isolating the system from vibrations or the source itself through isolators (Harris 2002).
- reducing the response by changing the natural frequency, dissipating energy or adding an auxiliary mass that oscillates out of phase with the system (Harris 2002).
- employing an active cancellation method (MIT OpenCourseWare 2013).

The system may also be dampened. Damping is the dissipation of energy which decays the amplitudes of free vibrations (Harris 2002). The transmissibility, which is the ratio of the system displacement to an external displacement, is represented on the vertical axis in Figure 13. The horizontal axis is the frequency ratio, r :

$$r = \frac{\text{Excitation Frequency}}{\text{Natural Frequency}}$$

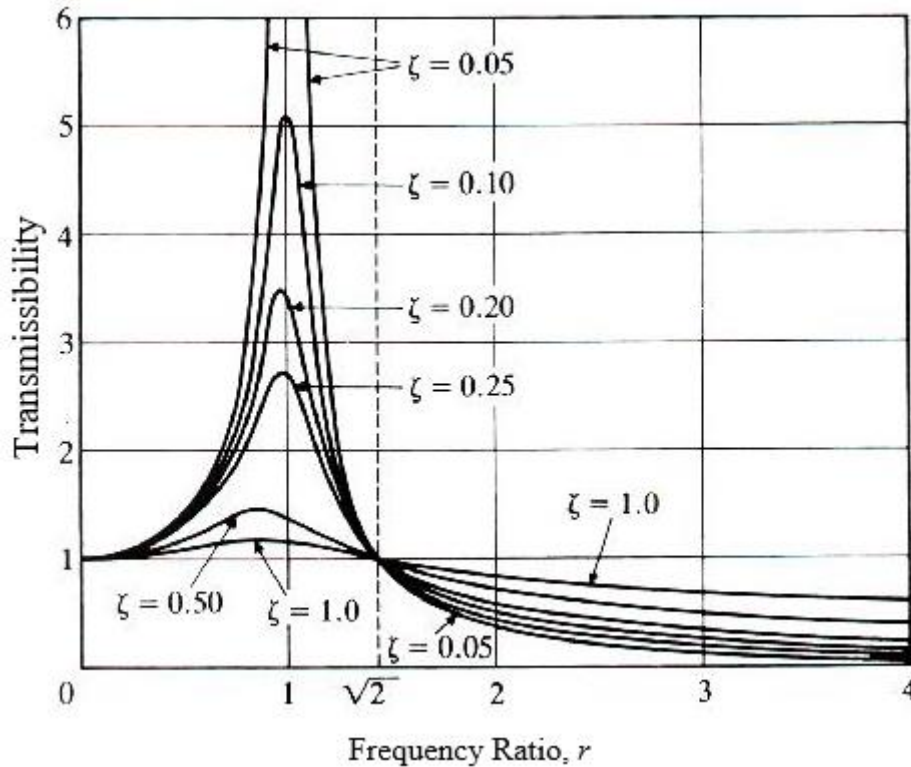


Figure 13: A plot that demonstrates the relationship between transmissibility, damping ratio, and frequency ratio (Friedrich 1998).

The damping ratio, ζ , is the ratio between the actual damping coefficient of the system and the critical damping coefficient (Harris 2002). Where critical damping is defined as the means of returning a displaced system to equilibrium without oscillation (Harris 2002).

To dampen the vibrations from a set excitation frequency, the greatest effect of damping occurs when the value of the frequency ratio is greater than $\sqrt{2}$ as presented in Figure 13. Thus, the natural frequency of the system may be manipulated by altering its stiffness and mass, to minimize the transmissibility of displacement. In addition, the damping ratio may also be altered by adjusting the damping coefficients.

However, caution must be taken. Certain appliances such as a motor, when it accelerates from rest, the excitation frequencies will be lower and thus the system will have to pass through a resonance zone. Should the excitation frequency and natural frequency remain similar for an extended period of time, the transmissibility will increase.

Design Process

Data Collection

Firstly, information on the PWC operating conditions had to be obtained. Of interest was the magnitude of forces exerted on the MC box, their directions, and frequencies.

Accelerometer

The typical accelerometer may not be implemented given the fact that it requires a computer connection. This is not a feasible approach to data collection when on the water. The solution was to employ an accelerometer that may be powered and store data, independent of a typical computer.

This accelerometer complication was addressed by implementing an Arduino Uno, a microcontroller (Arduino 2018), which served as a minicomputer. The Arduino was coded to receive inputs from the accelerometer and output the data into a Data Logging shield, see Figure 14. The code for the Arduino was compiled from two libraries, one for reading the accelerometer (Github, Inc. 2018) and the other for data logging (Adafruit n.d.). This code was then altered to cater to the needs of this project (**Appendix 1**). The shield had an SD card slot, where data was saved as a CSV file.

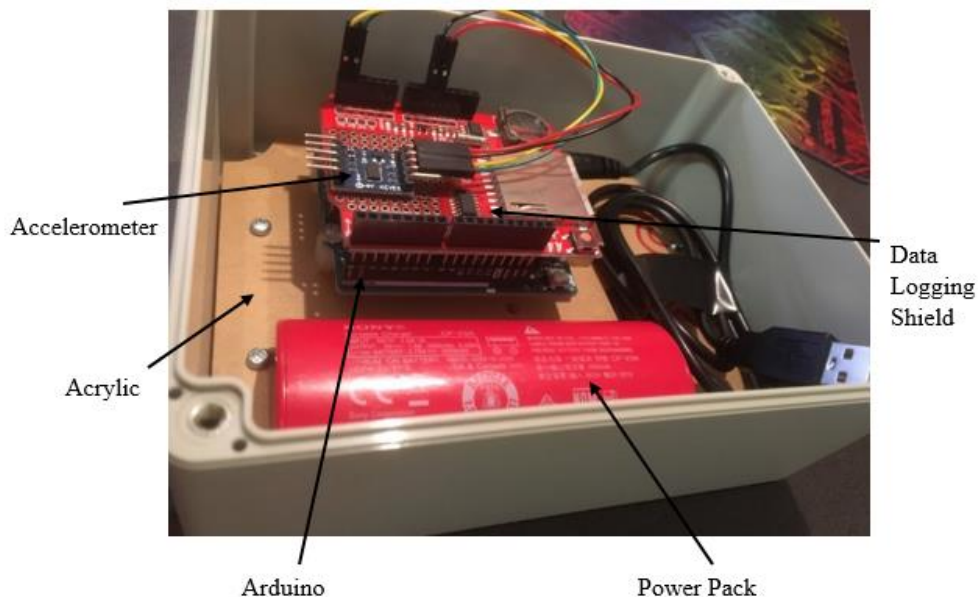


Figure 14: The arrangement of the accelerometer, the data logging shield, the Arduino Uno, and the power source.

The ADXL345 accelerometer is a 3-axis instrument that records within different thresholds, namely: $\pm 2g$, $\pm 4g$, $\pm 8g$, $\pm 16g$. It records over a 10-bit resolution range (Analog Devices 2009). This means that the recorded values presented span over a range of 1024 (which stems from: 2^{10}), from -512 to 512. These numbers map to the range of the set threshold, and values in between may be converted to its equivalent gravitational acceleration values through linear interpolation.

Recording Process

When it came to field testing, the Arduino was connected to the power bank (5V). At this point, it has started to record data. With the accelerometer box sealed shut, it would then be attached to the top of the MC lid through Velcro strips. The positive X-axis of the accelerometer was pointing portside, the Y-axis to the bow, and the Z-axis vertically upwards.

At this point the PWC was being sealed by putting in place its final exterior attachments prior to departure from the laboratory. Thus, the data for the first five minutes was discarded as the readings from putting the accelerometer box in place do not represent the accelerations of the MC box. During those five minutes the PWC was stationary, and it is only shortly after this period that it starts being transported to the river. The same is done upon its return.

It should be noted that the accelerometer was recording data throughout its voyage to the testing site, as the MC was still subjected to shocks and vibrations when the PWC was being towed. Once the PWC carried out its test rides it is brought back to the laboratory.

Field Data Processing

There was no reason to calibrate the accelerometer to read zeros at a new resting position/orientation. The reasoning behind this was because of the human error which occurs when the accelerometer box was taken from the PWC and replaced between test trials. Unless the user could put the accelerometer box back in the exact position without the slightest discrepancy, there is no point to calibrate it. This is because a slight change in its orientation from the set resting position would read nonzero values. The solution instead was to note the resting position values and adjusting the readings when data processing.

From these field tests, the Arduino setup records three columns of raw data (three axes). The mode was obtained for each column to find the zero point of reference, see Table 1.

Raw Data			Resting Position			Calibrated Readings (m/s ²)		
x	y	z	x	y	z	x	y	z
-6	-10	130	-8	-13	130	0.15328	0.22992	0
-6	-11	130				0.15328	0.15328	0
-6	-11	129				0.15328	0.15328	-0.0766
-7	-10	130				0.07664	0.22992	0
-6	-10	130				0.15328	0.22992	0
-6	-11	129				0.15328	0.15328	-0.0766

Table 1: a sample of the data to highlight the data processing.

The acceleration values were obtained through the following equations, which accounts for the calibration and change of units:

$$\text{Calibrated Reading} = \text{Raw Data} - \text{Resting Position}$$

This *Calibrated Reading* was still unitless and cannot appropriately represent a physical system. The goal was to obtain a calibrated reading which had units of (m/s^2) . Intuitively, the ratio of the dimensionless calibrated reading and the upper bound of the accelerometer (512 as per the 10 bit resolution), was equal to the calibrated reading (m/s^2) divided by the set upper threshold ($2g, 4g, 8g, 16g$). From the field test, the upper threshold was $4g$.

Thus,

$$\frac{\text{Calibrated Reading}}{\text{Upper Bound of Accelerometer}} = \frac{\text{Calibrated Reading} \left(\frac{m}{s^2}\right)}{(\text{Upper Acc. Threshold}) \times (\text{Gravity Constant})}$$

$$\text{Calibrated Reading} \left(\frac{m}{s^2}\right) = \frac{(\text{Calibrated Reading}) \times (\text{Upper Threshold}) \times (\text{Gravity})}{\text{Upper Bound of Accelerometer}}$$

$$\text{Calibrated Reading} \left(\frac{m}{s^2}\right) = \frac{(\text{Calibrated Reading}) \times 4 \times 9.81}{512}$$

For the first x value:

$$\text{Calibrated Reading} \left(\frac{m}{s^2}\right) = \frac{(-6 - (-8)) \times 4 \times 9.81}{512} = 0.15328 \frac{m}{s^2}$$

The threshold for the accelerometer was set to $4g$ was because the highest resolution was sought without exceeding the threshold. During the first trial, the threshold was set to $2g$. However, whilst it gave more accurate readings over the range of $-2g$ to $2g$, the threshold was exceeded. However, the exceeded value simply reads as $2g$, which does not represent the reality. It was found that with $4g$, acceleration values did not exceed the threshold, and thus this was the most accurate threshold that may be set. Readings were taken every quarter of a second to ensure that the number of data points to process would not be extremely large, and to reduce the time between each reading.

These acceleration values were smoothed out by a three-point moving average. Simply, the first three data points were averaged to create one new data point, and so on. The reason for this was because the impacts of outliers would be reduced, but still present to maintain a conservative approach in the design process.

The smoothed acceleration values were plotted against time, with the same range on both axes for ease of a visual comparison, see Figures 15, 16, and 17.

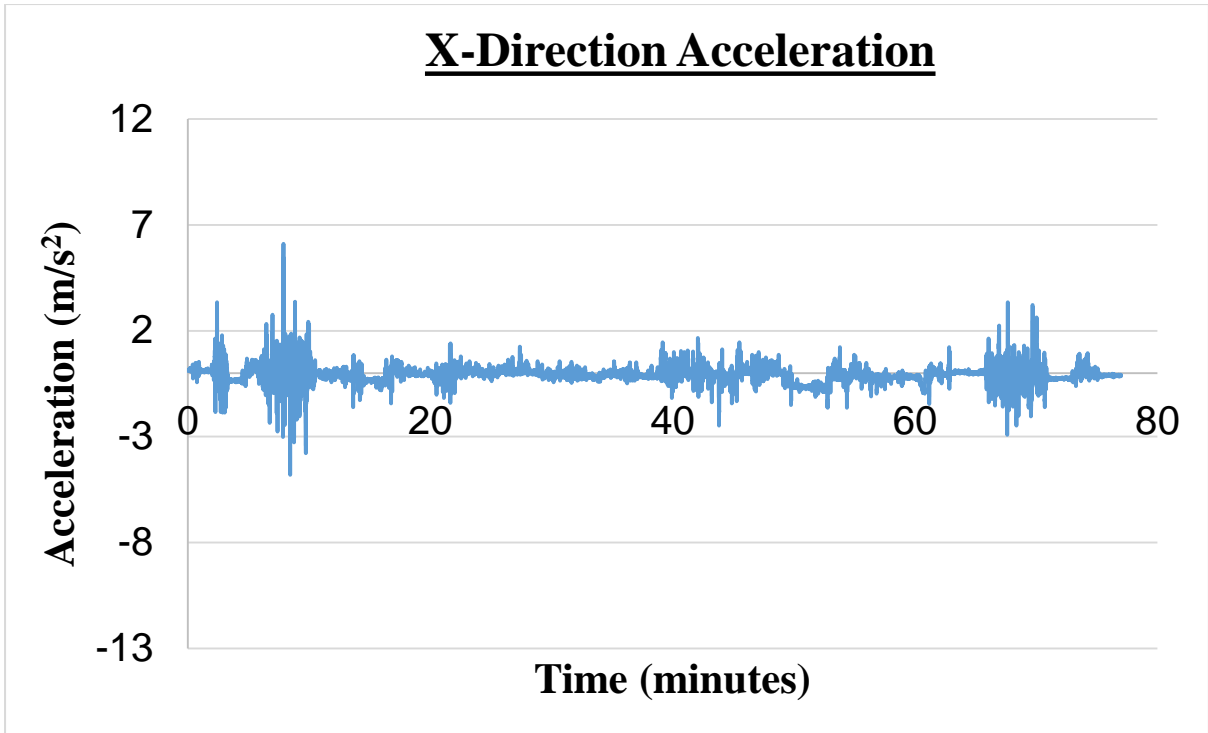


Figure 15: The variation of acceleration in the X-direction over the duration of the field test.

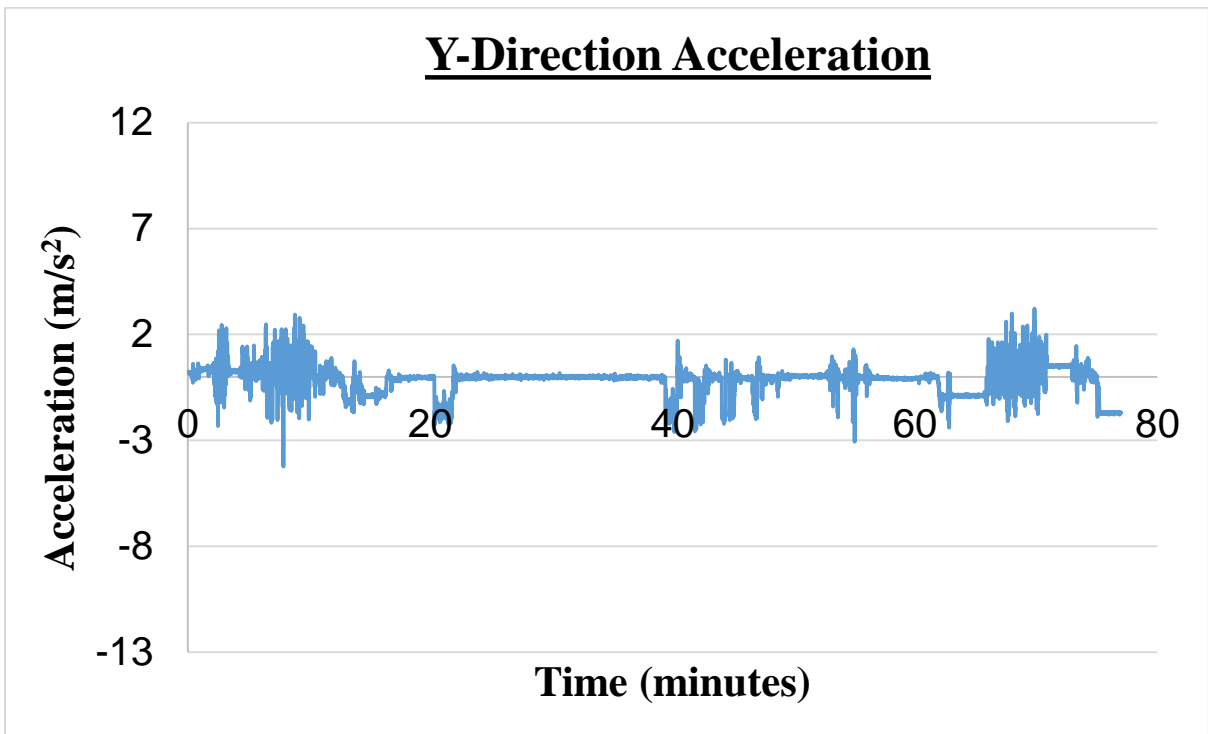


Figure 16: The variation of acceleration in the Y-direction over the duration of the field test.

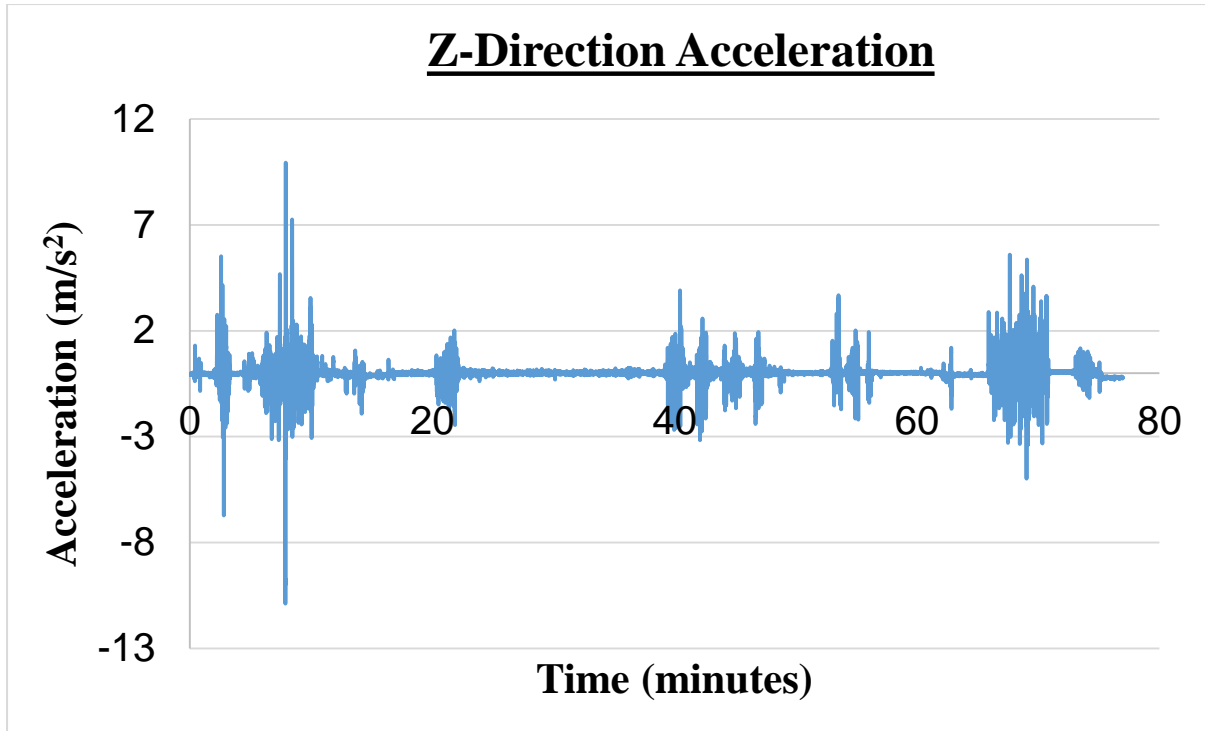


Figure 17: The variation of acceleration in the Z-direction over the duration of the field test.

It is immediately evident that the Z-axis experiences the largest accelerations, and thus, one would associate with it the largest forces. In a design perspective, this finding highlights the fact that the mount should focus on shock absorption in the vertical axis.

In terms of forces, the actual acceleration values were employed, not the smoothed, for a more conservative approach. The maximum acceleration values were obtained by simply extracting the maximum for each axis. Once again, to reiterate the difference between the actual acceleration, and the smoothed, this is presented in Table 2.

	Max Acceleration (m/s ²)		
	x	y	z
Non-smoothed	15.7113	5.82469	24.9848
Smoothed	6.1057	3.21891	9.93773

Table 2: The comparison of maximum accelerations for non-smoothed and smoothed data.

It should be made clear that these accelerations represent the behaviour of the MC box. However, an assumption is made such that all components in question behave in the same manner for the purposes of the designing process.

These accelerations were converted to forces by multiplying it to the mass of the MC box and its plate (24.5kg), as per Newton’s Second Law:

$$Force = Mass \times Acceleration$$

The force may be converted into an equivalent load by dividing it with the gravitational constant:

$$\text{Equivalent Load} = \text{Force} \div \text{Gravitational Constant}$$

This is presented in Table 3 for both the MC box and the mass of the other components (fuse box and others), which will be situated on a separate plate (7kg).

	x	y	z
Maximum Force (N) for MC	385	143	613
Equivalent Load (kg) for MC	40	15	63
Maximum Force (N) for lighter components	110	41	175
Equivalent Load (kg) for lighter components	12	5	18

Table 3: The maximum forces experienced by components from the field test.

Thus, the mount must be able to withstand forces of greater than those presented in Table 3.

Design Options

Active & Passive Isolation Systems

There are two distinct types of vibration isolation systems: active and passive (Polymer Technologies 2014). Active systems require sensors to detect oncoming waves or road features. These sensors will then feed this information into a circuit board, which will command actuators to produce a counterforce to the shocks. The benefit of this system is that it will address all frequency ranges in question and remove all vibration or shock amplitudes (Accurion 2018).

However, an active system will increase the complexity. For the purposes of this project, there are simpler methods. An active system will most likely exceed the set budget. Most importantly, there will be an additional power draw on the batteries. From the field tests, when the PWC was operating at full throttle, the ride time was ten minutes. Given that the PWC is an entertainment product, it would not make economic sense to further dwindle the already low ride time; especially if it is in exchange for an active isolation system, when a passive would be sufficient. One might argue that an additional power source may be added into the PWC. However, PWC already sits low in the water and added mass would increase its drag.

A passive system depends solely on the natural reaction of materials and objects. Typical passive isolation components include rubbers and springs. These are significantly cheaper, it also keeps the complexity of this project to a reasonable level with no power draw.

To further stress the comparison, a common example of an active vibration isolation system is noise cancelling headphones. The user experiences a reduction in noise as the headphones are emitting soundwaves that superimpose with external soundwaves to cancel amplitudes (Audio-Technica 2018). These headphones require power, more skill in its creation, and are expensive. Earmuffs would be the equivalent passive isolations system which absorbs external

soundwaves through its materials. They are a fraction of the cost, require no power of usage, and are much easier to produce.

Passive Isolation Options

Shock Absorber

In cars, shock absorbers serve to reduce the transmission of energy from the road feature to the driver and prevent prolonged oscillations. Absorbers (Figure 18), convert mechanical energy to thermal energy through viscous effects. Absorbers contain highly viscous fluids, the fluid resists compression, which causes friction as it passes through the constriction within (Quora 2016). Its resistance to compression prevents continued oscillations.



Figure 18: A pair of shock absorbers (Shock Absorber n.d.).

Springs are installed to return the absorber to the equilibrium position.

Advantage

Shock absorbers have proven their effectiveness in the automotive industry, it is a tried and tested solution.

Disadvantage

Prices range from roughly \$50 to \$200 each. A feasible design would require more than one absorber.

Springs

Springs are often associated with vibration and shock isolation. The displacement of the spring from its equilibrium position renders a restoring force. This is represented by Hooke's law (Williams 2015):

$$Force = -(Spring\ Stiffness, k) \times (Displacement, x)$$

The restoring force is denoted by the negative sign, and the spring stiffness is an intrinsic property of the spring (Newtons per metre).

Advantage

The cost of springs is low, allowing for several different types to be purchased and tested for suitability.

Another advantage is that the spring returns to the equilibrium position due to the restoring force. The spring absorbs energy by compressing from the shock, and converts it into potential energy (PE):

$$PE = \frac{1}{2}kx^2$$

(LearnThermo n.d.)

Disadvantage

However, this restoring force and its displacement causes continued oscillations. Should another external shock be applied to the system whilst these oscillations are ongoing, the amplitude of these displacements could increase. In addition, a spring system implies that the components are somewhat mobile, which is not ideal for the operating conditions.

Bobbins

Bobbins are a type of rubber mount. They are cylindrical and may be attached to mechanical fasteners such as bolts. Bobbins come premade with threaded holes to receive a bolt, male versions are also available, as well as a combination of the two, see Figure 19.



Figure 19: Various types of bobbins (Chains & Drives 2018).

Advantage

Bobbins are inexpensive and come with various fastener combinations. This increases the possible design options and could therefore simplify the mounting system.

Disadvantage

Given that the bobbins do not have a continuous hole throughout the rubber cylinder, and have threaded holes, it implies that it will experience tensile loads. It should be noted that the metal plates are only discs present on the face, serving to distribute axial forces. Thus, these do not occupy much space in the cylinder. This means that the bolts serve as connectors, but the rubber is the absorber. In compression this is no issue, however, rubbers often fail when subjected to tensile forces. For example, a rubber band does not fail when scrunched up (compressed) but

will begin to tear, and ultimately snap, when stretched (tensile load). Hence, bobbins may not be the ideal solution as they may fail when the PWC proceeds from a wave crest towards the trough. In that situation, the components would accelerate upwards, and the bobbins would be loaded in tension.

Rubber Mounts

Rubber mounts are often implemented as a means of isolating the ground from vibration machinery such as extraction fans or generators. These often act as ‘feet’ to the machinery (Figure 20). The top surface has a steel plate under the rubber, likewise for the flat bottom section. This allows for bolts and screws to secure the rubber mounts and the machinery together, and to the ground.



Figure 20: Rubber mounts that act as ‘feet’ for vibrating machinery (Embelton 2011).

Advantage

Rubber mounts have proven their effectiveness by isolating the ground from various vibrating machinery. They are also relatively inexpensive. Despite its slight resemblance to bobbins, it avoids the issue with tension. This is achieved by its hole in the centre, which passes through. Although the hole is threaded, by simply selecting a bolt that is too small to bite, the issue is resolved.

Disadvantage

The steel on the interior of the rubber mounts is still exposed to the operating environment. Humidity and water could cause the metal to rust, over time it may compromise the structure of the rubber mount. This would need to be addressed with either a preventative measure or regular checking and maintenance.

Rubber Mats

The initial plan was to employ a rubber mat in the design. Rubber mats are often used as an additional layer of flooring to protect the ground from dropped objects, in the gym for example.

Advantage

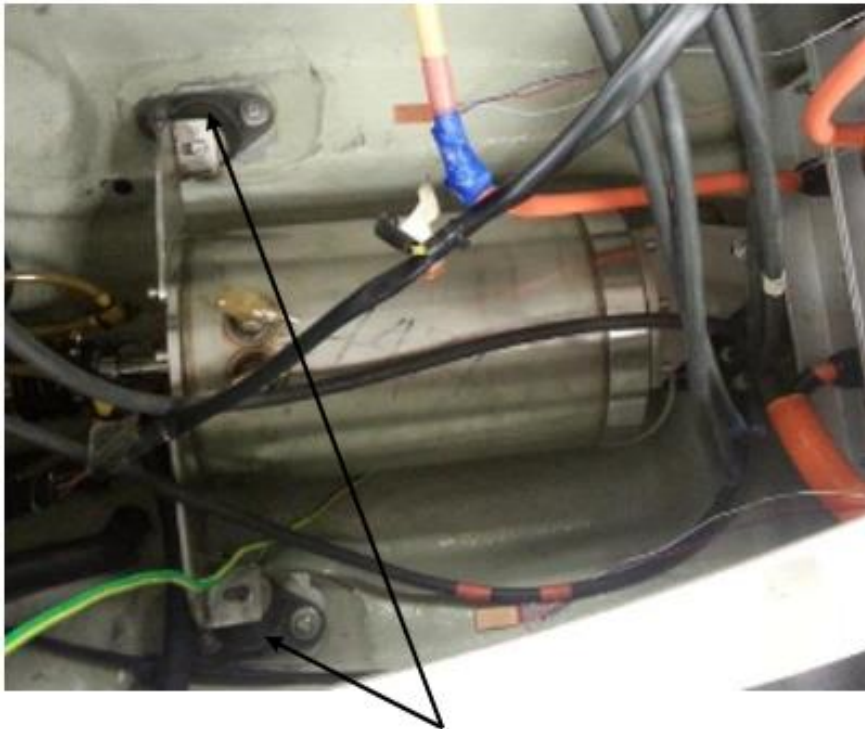
Rubber mats are low in cost, in addition, its large surface area allows for a more even distribution of shock.

Disadvantage

Rubber mats may be an effective solution; however, it would be challenging to incorporate it into the design. All the other design options may be fastened in some way to the plate. The mat may be adhered, or potentially sandwiched between two plates. Although this may be a viable option, there are more appropriate solutions available.

Design Option Selection

By comparing the advantages and disadvantages of the above design options, it became apparent that the rubber mounts were the most appropriate choice for this project. Its low cost would allow for the purchase of different rubber types, as sets. Each set could therefore be tested for its suitability to the mass of the components. In addition, it is a tried and tested method. It is also extremely applicable in the context of the PWC, as the motor itself utilizes these rubber mounts to isolate the PWC from its vibrations, see Figure 21.



Motor Rubber Mounts

Figure 21: The motor is mounted of rubber mounts to isolate the PWC from its vibrations (Jensen 2015).

However, in the design, it must account for the tension issue, and consider corrosion preventative measures. A total of three sets were purchased from Embelton, a company that specializes in noise and vibration isolation. According to the Embelton specification sheet, the rubber mounts behave close to a linear relationship from 10% to 100% for axial loads (Embelton 2011). Thus, its spring stiffness may be approximated as per Hooke's law. Each set consists of four of the same rubber mounts, with varying rubber hardness between sets. This is presented in Table 4 below.

	Maximum Axial Load	Axial Deflection	Spring Stiffness, k	Maximum Shear Load
Colour	[kg]	[mm]	[N/m]	[kg]
Blue	17	5	3400	5.67
White	25	5	5000	8.33
Green	55	5	11000	18.33

Table 4: Readings per single rubber mount (Embelton 2011).

A range of different load capacities were purchased for testing purposes. Given that this project concerns two separate accumulated masses, 24.5kg, and 7kg, softer rubbers may still be applicable. The 7kg system represents the accumulated mass of the smaller components such as the fuse box, throttle box, and bender module.

From now on, each set will be referred to by its colour: Blues, Whites, and Greens; with Blues being the softest, and Greens as the hardest.

Mount Design

With the rubber mounts acquired, the final phase of the design may commence. Embelton has a recommended means of attaching the rubber mounts, see Figure 22.

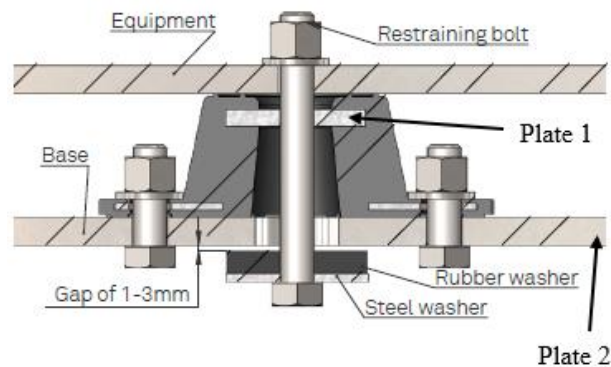


Figure 22: The recommended means of employing the rubber mounts (Embelton 2011).

However, after discussing the tension issue with their engineer, it was their professional opinion to bypass the rubber mount thread by utilizing a smaller diameter bolt. The concept is such that the rubber would take the load in compression, and the bolt would take the load in tension. With a base recommended mounting system, and a solution to the tension issue, the next step was to determine how the rubber mount would be attached to the PWC.

As established earlier in the literature review, previous students that mounted the MC had fastened it on top of the motor, likewise for the latest battery. Given that no holes can be drilled into the fiberglass, an adhesive must be employed. It was decided that structural wooden blocks would be adhered to the PWC as it is a softer material to shape than metal.

It must be acknowledged that Plate 2 in the recommended mounting system (Figure 22) does not exist yet for the PWC. The purpose of Plate 2 is to prevent the rubber mounts from taking any tensile loads. Without it, the bolt head would be positioned under the Plate 1, and thus the rubber would experience tension.

Thus, the rubber mounts would be screwed into the adhered wood with a plate placed in between the two to act as Plate 2. The MC plate would sit on top of the rubber mounts (one per corner) and secured in place by bolts that bypass the thread of the rubber mounts. The MC box would be bolted to its plate as per usual. This arrangement is displayed in Figures 23 and 24.

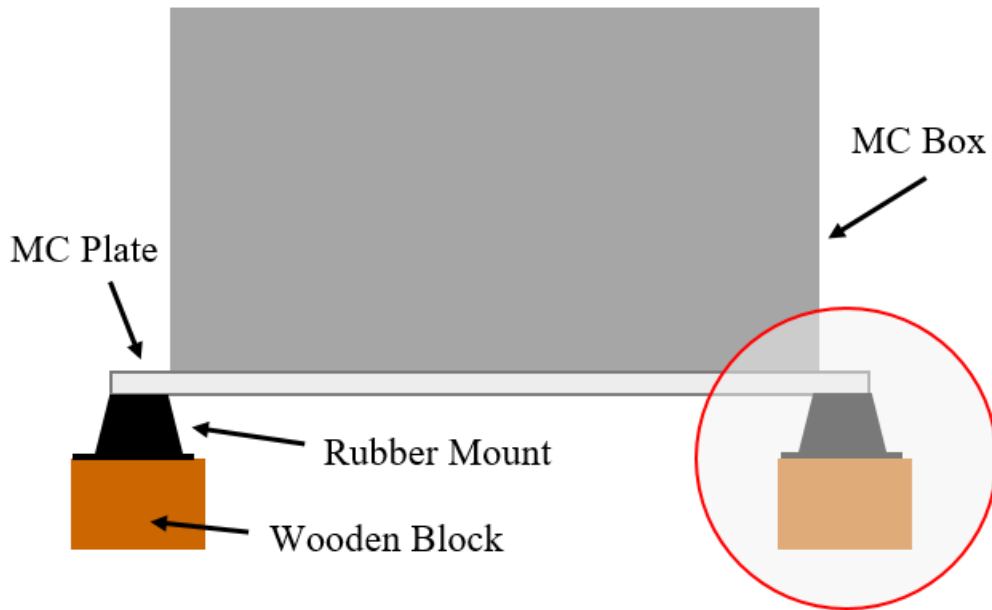


Figure 23: An overview of the MC mounting system, with a rubber mount on each corner of the plate.

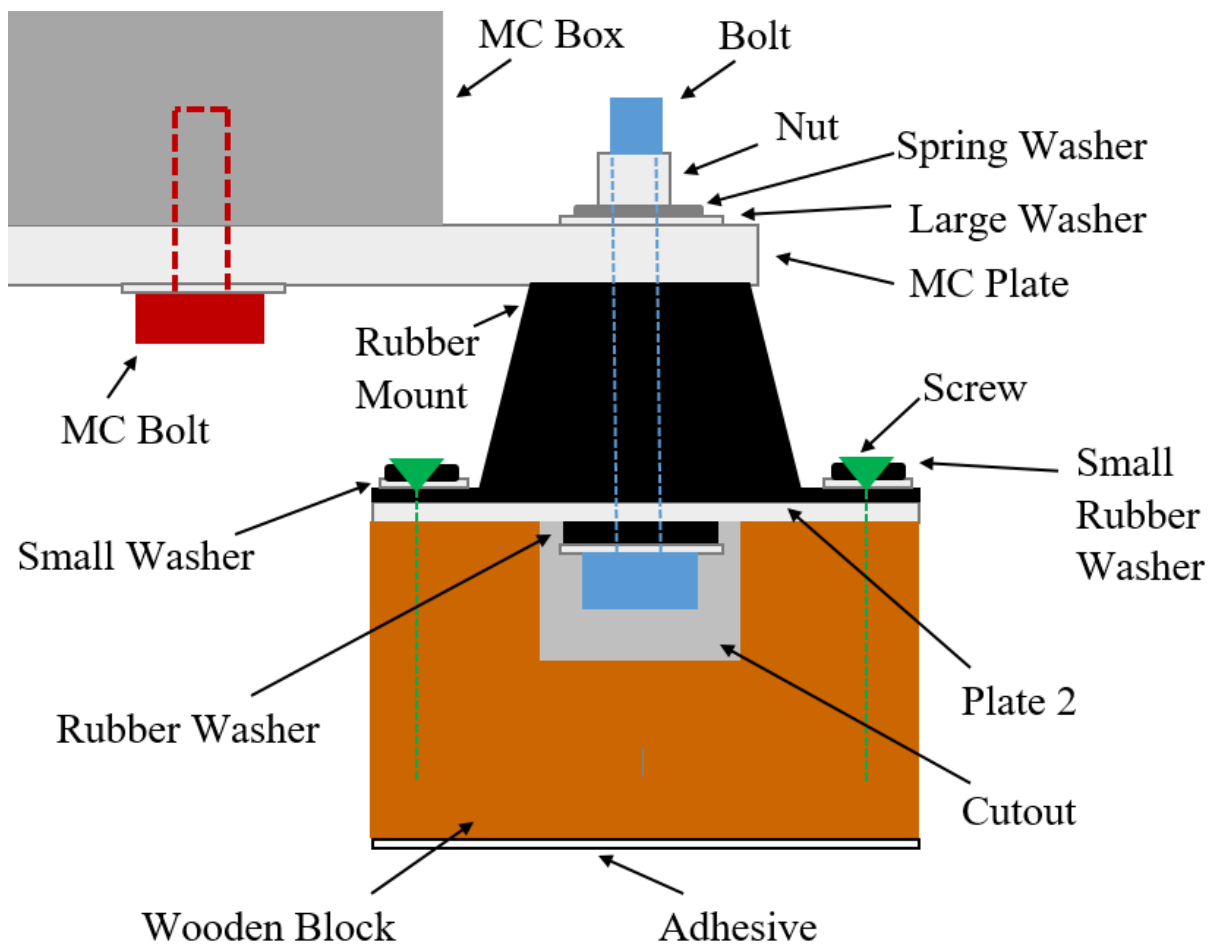


Figure 24: A zoomed in sectional view of the red circle in Figure 23.

The sole difference for the 7kg mass system in terms of its mounting is how it is attached to its own plate. For the MC box, it is bolted. However, to address the customization criteria and the convenience of mounting, Velcro strips were implemented for these lighter components. This plate was constructed out of aluminium and cut into shape to fit the internal shape of the bow closely.

Material Selection

The necessary parts were selected based on their material properties, with an emphasis on corrosion resistance. These are outlined below:

Structural Wood

Structural Pine was selected for its strength; however, it would require a form of coating to protect it from the operating conditions, or it would eventually rot.

Spray

Cabot's Exterior Clear Marine Grade spray was selected based off its superior resistance to mould and dirt, but also its suitability for outdoor use.

Aluminium Plates

Both the MC and 7kg mass system plate are aluminium, which is resistant to corrosion due to its protective oxide layer (Knight 2014).

Adhesive

Gorilla Wood Glue was selected for the strength of its bond, and because it is suitable for both indoor and outdoor use. It is also water resistant.

Screws

The galvanized steel screws are suited for timber and have a small rubber washer on it to prevent water from entering from the outside. This type of steel is also resistant to corrosion (Wenzel Metal Spinning n.d.).

Bolt

The bolts were coated with yellow zinc to resist corrosion (Total Materia 2002).

Washers

Small washers for the screws, large washers for the bolts, and spring washers for the nuts are all zinc plated to provide resistance to corrosion (Total Materia 2002). The rubber washers may need replacing every few years should they deteriorate.

Rubber Mounts

The specification sheet states that the metal components within the rubber mounts are protected from corrosion (Embelton 2011). It would be good engineering practice to occasionally undergo a visual inspection.

Testing Frame

With the three rubber sets, it was a matter of selecting the appropriate set for the different mass systems through laboratory testing, the 24.5kg and the 7kg. The first step was to construct a testing frame instead of borrowing a vibration table. The justification behind this decision was that less external factors, such as resistance to borrowing the equipment, its availability, and paperwork, could delay the testing.

The second reason for constructing the testing frame was to verify the design physically. It is not uncommon for design aspects to be overlooked and are only acknowledged when the design had been physically created. The testing frame also served in part as a prototype for the mount.

The testing seeks to compare the behaviour of the different sets when exposed to the same force and mass system. From there, the findings were analysed and the results compared to determine the most suitable sets.

The testing frame was designed to allow for the delivery of a consistent force. There are complicated and expensive means of delivering a consistent force, however the most convenient and inexpensive method is to conduct drop tests. The testing method, however, is constrained. It would be unwise to drop expensive equipment and record its response. Thus, the testing frame was designed as per Figure 25.

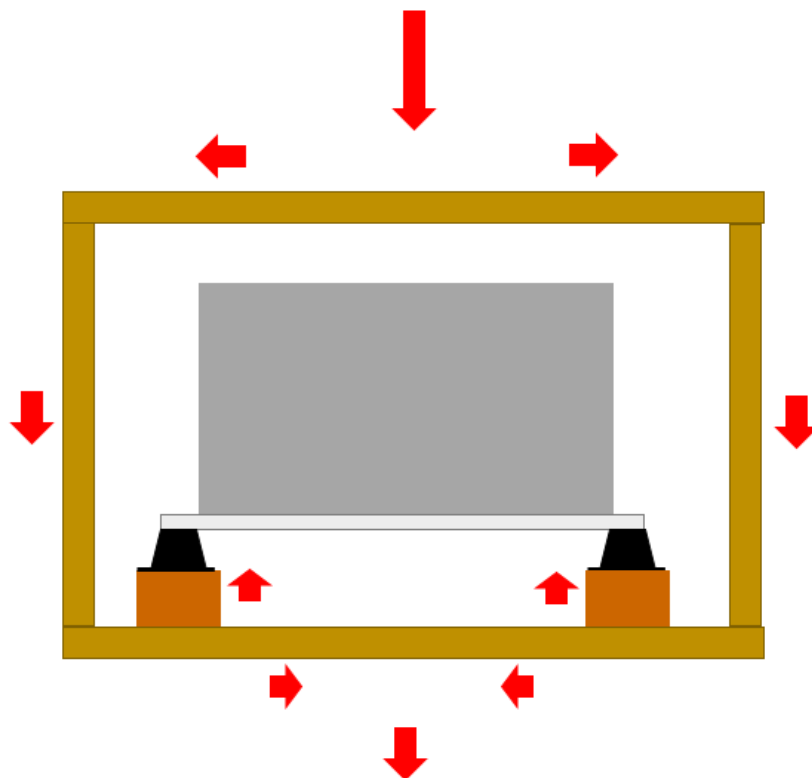


Figure 25: The red arrows represent the transmission of shock from the initial applied load. The shock is transferred through the frame. At the bottom, part of it leaves the system by entering the ground and the other ascends through the mount.

The concept was to apply a force on the top surface. This force would be transmitted through the columns and enter the base. The shock and vibrations would then ascend through the mounting system, with part of it dissipating through the ground. This testing allowed for a more controlled procedure that did not compromise the safety of the components.

Consistent force may only be achieved by dropping a mass from the same height and angle of incidence repeatedly. This mass was also be spherical so that there was only one point of contact.

Testing Procedure

Prior to testing, three initial trials were run. The same accelerometer system was employed, however with no delays between its sampling. From these trials, it was determined that the maximum sampling frequency of the accelerometer was slightly lower than 71Hz. This implies that frequencies of only up to 35Hz may be accurately measured by the accelerometer. This is in accordance with the Nyquist Theorem which is explained in **Appendix 4**. Although limited to 35Hz, this is still valid as wave frequencies are relatively low and will not exceed this threshold. This is because the worst-case scenario is when the PWC collides with oncoming waves at full speed. However, the maximum velocity of the PWC is approximately 30km/hr from the latest field test. Thus, it is intuitively impossible for the PWC to experience 35Hz from waves of significant size. Hence, the information sought from these tests was to determine which of these sets, for the different mass systems, will have the lowest excitation for the range of 0 – 10Hz, and have the greatest maximum shock absorption.

The first mass system was the MC box with its plate. This was installed into the testing frame, and the accelerometer was attached directly onto the MC with a Velcro strip, see Figure 26.

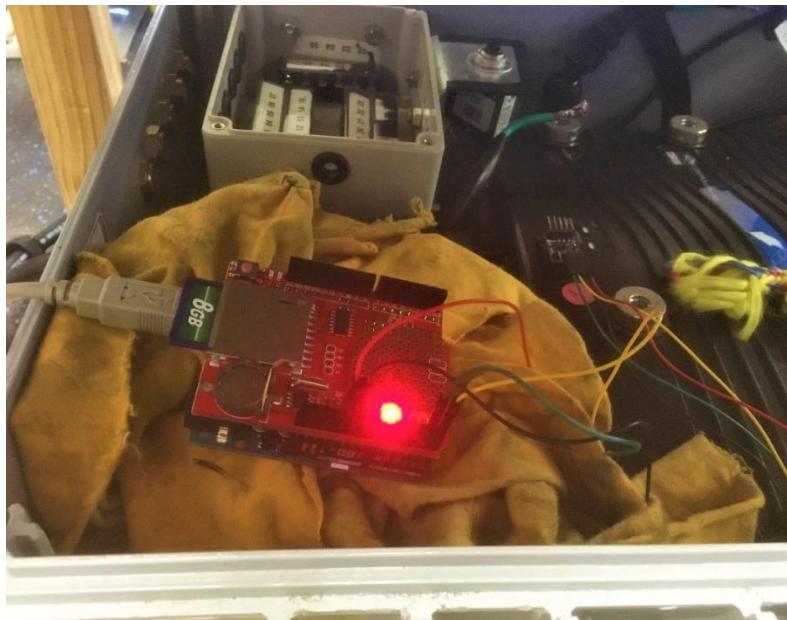


Figure 26: The Arduino system was placed on a rag to isolate it from the shocks, the wires lead to the accelerometer, attached to the MC.

There were four types of tests, with each test consisting of 10 trials. Each trial was the application of a force by dropping a spherical mass from a set height. It was allowed to collide with the testing frame once and was caught prior to making contact again. Once the shocks have dissipated, a few seconds later the force is applied again. The force was sufficient to provide recordable vibration, and not enough to cause damage.

The first test was the control test, where no rubbers were installed. The remaining three were with the different rubber sets. These tests were repeated on the second mass system (7kg). However, given that certain components within the PWC could not be extracted without great difficulty and repair, an alternative had to be employed. A box identical to the fuse box was filled with mass until it was 7kg, testing was conducted with this instead, see Figure 27. From these tests, the same parameters of data were obtained as per the field test.

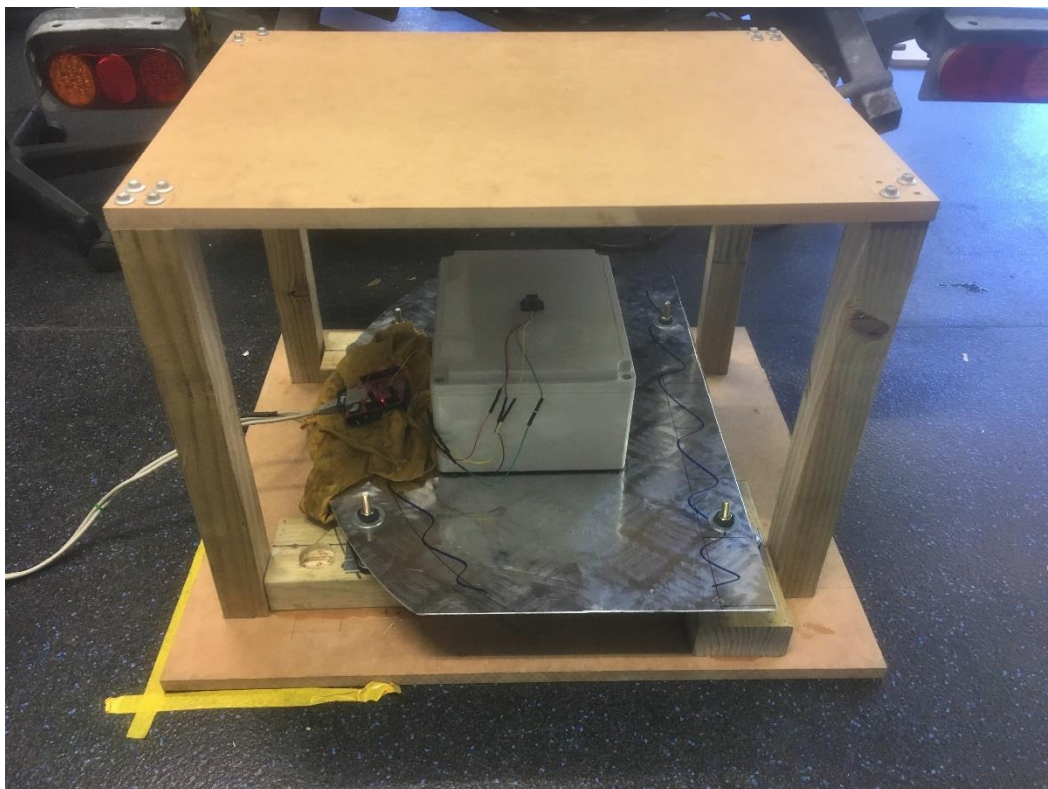


Figure 27: The testing setup for the lighter components mass system, with the testing frame.

Data Processing

The primary step in data processing was to extract the ten trials from each test. These trials were denoted by a sudden spike in the accelerometer readings. A total of 71 data points were taken per trial, which was equivalent to a duration of one second. The spike of each trial was situated in the middle of the range, with equilibrium readings at the beginning and end of this extracted range. This was to ensure that the important data was captured within each trial.

Once all ten trials had been extracted for each test, the remaining data would only consist of equilibrium readings and thus serve no purpose. Each trial then had its data smoothed with a three-point moving average. As a result, each trial now has 69 data points. There are two reasons behind smoothing the data, the first was to reduce the ‘noise’ of the data so that when a Fast Fourier Transform is applied to the data, it would for the most part represent the frequency of the mounting system. The second was to obtain more consistent results when analysing the maximum response of each rubber mount.

Average Maximum Response

The purpose of the maximum response was to determine which of the rubber sets absorb the most energy for the given mass system. The ideal set would be the one with the lowest average maximum response acceleration readings.

For each trial, the magnitude of the smoothed data was obtained. Then, the maximum of the magnitudes was extracted. For a given test, these maximum response values were averaged. This number would therefore represent the average maximum response for either the control test, or one of the rubber sets. This average maximum response was conducted for all three axes and for both mass systems. The summarized results are available in **Results & Discussion**.

Fast Fourier Transform

The purpose of performing the Fourier Transform was to reveal at which frequencies the mounting system was excited. This would vary depending on the rubber set installed, and thus allows for a visual comparison.

To accomplish this, a MATLAB code was created (**Appendix 2**). The Fast Fourier Transform (FFT) was performed on each trial. The Transform ultimately yielded a vector plot over a frequency range. The average FFT of a test was the average of this vector for each trial within that test. This was carried out for the control test, and the three rubber sets. It was conducted for all axes and both mass systems. The findings are presented in **Results & Discussion**. The Fourier Transform is fully explained in **Appendix 4**.

Results & Discussion

Based off the initial field test, the data suggests that the axis with the greatest excitation was in the Z-direction. Thus, the decision-making process for selecting the appropriate rubber set will prioritise the Z-axis over others. The X-axis experienced significantly less than the Z, however, it had greater excitation amplitudes than the Y-axis. Hence, the Y-axis has the lowest weighting in the decision-making process.

Also, given that each set has four rubber mounts, the total force that each set may withstand are as follows in Tables 5 and 6. Note that according to the specification sheet, the maximum shear force for each rubber is a third of the maximum axial load (Embelton 2011).

Field Test Axial Load for MC	Field Test Axial Load for Lighter Components	Set	Maximum Axial Load	MC Safety Factor	Lighter Components Safety Factor
[kg]	[kg]		[kg]		
63	18	Blue	68	1.08	3.78
		White	100	1.59	5.56
		Green	220	3.49	12.22

Table 5: Maximum axial loads experienced by components, compared to maximum axial loads that each set can withstand.

Field Test Shear Load for MC	Field Test Axial Load for Lighter Components	Set	Maximum Shear Load	MC Safety Factor	Lighter Components Safety Factor
[kg]	[kg]		[kg]		
40	12	Blue	22.67	0.57	1.89
		White	33.33	0.83	2.78
		Green	73.33	1.83	6.11

Table 6: Maximum shear loads experienced by components, compared to maximum shear loads that each set can withstand.

Already prior to the laboratory tests, Tables 5 and 6 indicate that all sets are suitable for axial loads, albeit that the safety factor for the Blue set is only 1.08 for the MC. However, the only set that may withstand the load of the MC in shear are the Greens. Having said that, the tests for the other rubber mounts were still conducted. This is to verify if there are any outstanding benefits of the Blue and White set. If so, it may be worth reconsidering the design and undergo another iterative process.

MC and Plate Mass System

Three Axes Average Maximum Response

Figure 28 presents the average maximum response of each set as a percentage of the control response. The averaged maximum response for the control test was obtained to be 17.04 m/s^2 . This value was set to 100% and the corresponding values from the other sets were converted to a percentage for easy comparison.

It is immediately evident from Figure 28 that the White set performed the best in the X-direction, with an overall reduction in excitation by 43% (or the lowest response of 57%). This was followed behind closely by Greens at 40.4%.

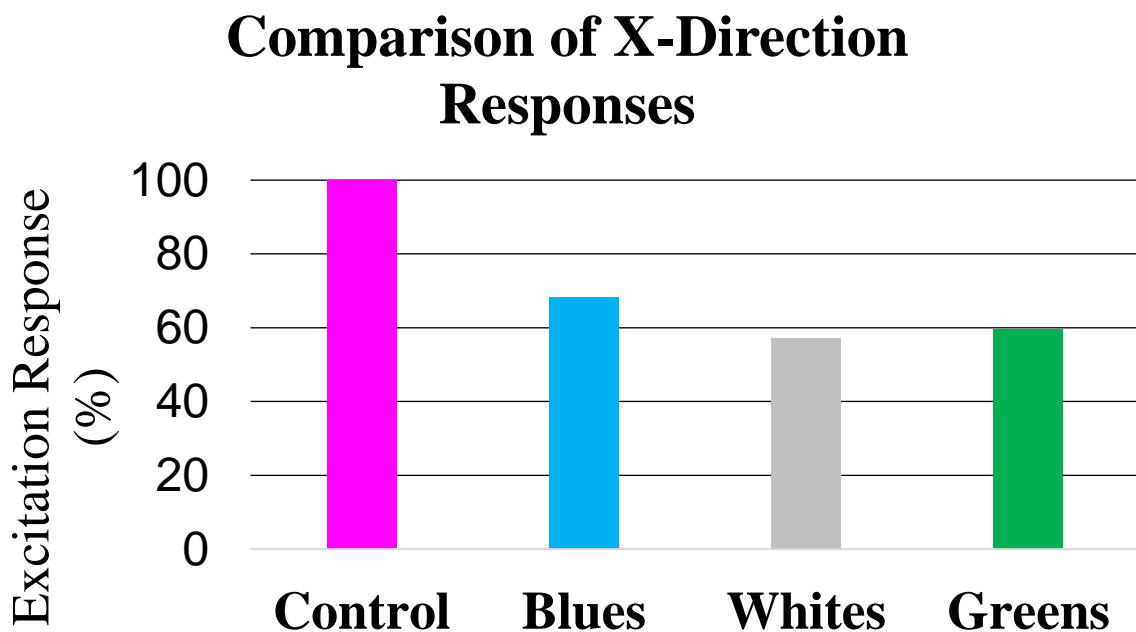


Figure 28: Average Maximum Response in the X direction for the MC system.

On the other hand, Figure 29 highlights the fact that the Greens accentuate the excitations. This implies that forces would be amplified by the Greens. In this case, by 13%. Blues on the other hand reduced the response by 41%.

Comparison of Y-Direction Responses

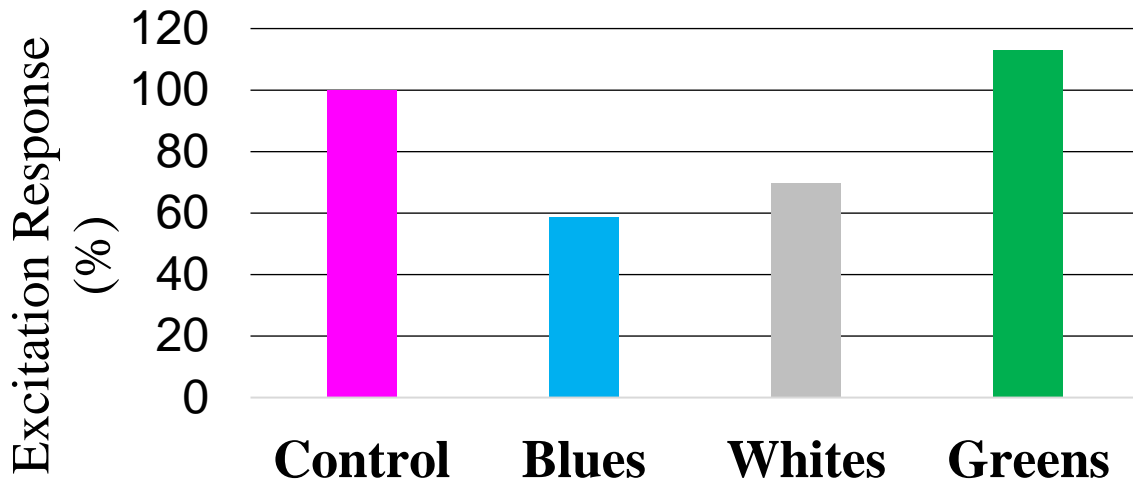


Figure 29: Average Maximum Response in the Y direction for the MC system.

In the Z-direction however Figure 30 reveals that the Greens are the ideal choice in reducing shock transmission. The reduction is by approximately 21%. It is worth noting that there is a relatively large differentiation between the performance of the other two sets when compared to Green in this axis. Blues and Whites reduce excitations by 10% and 11% respectively.

Comparison of Z-Direction Responses

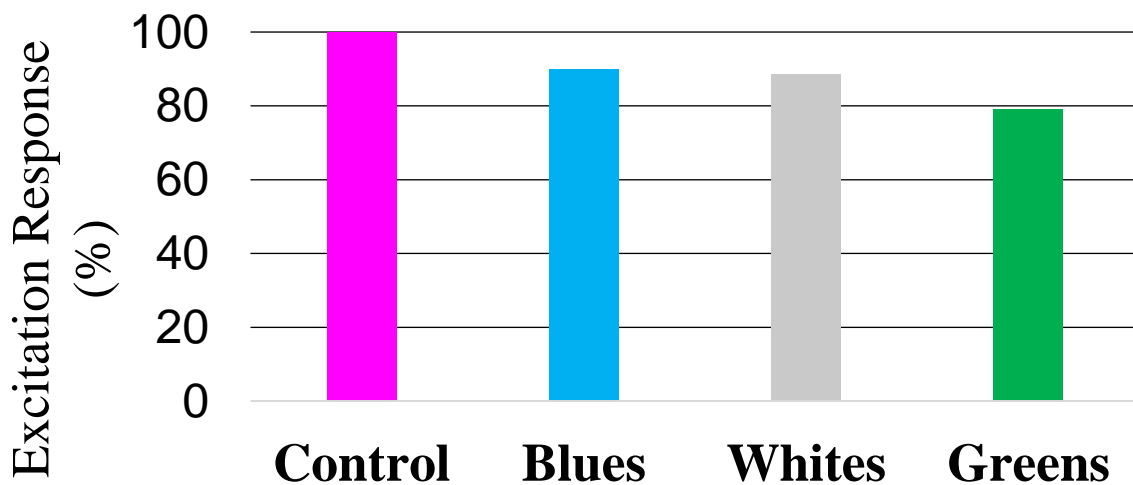


Figure 30: Average Maximum Response in the Z direction for the MC system.

Three Axes Fast Fourier Transform

Firstly, the frequency axis in Figure 31 is limited to 35Hz as explained with the limits of accuracy when sampling at a frequency of approximately 70Hz. Also, the vertical axis represents acceleration in decibels. The greatest importance in this analysis is the comparison between the same type of data (which has undergone identical processing). This consistency allows for a meaningful comparison with justifiable results. It is also worth noting that all tests do not reach the vertical axis. This is simply attributed by the 3-point moving average which removed the first two data points for each trial.

Beginning with the X-axis, it is immediately clear that the Greens outperform all the other sets for the lower frequencies. This indicates that Greens have the lowest response in the X-axis at those lower frequencies.

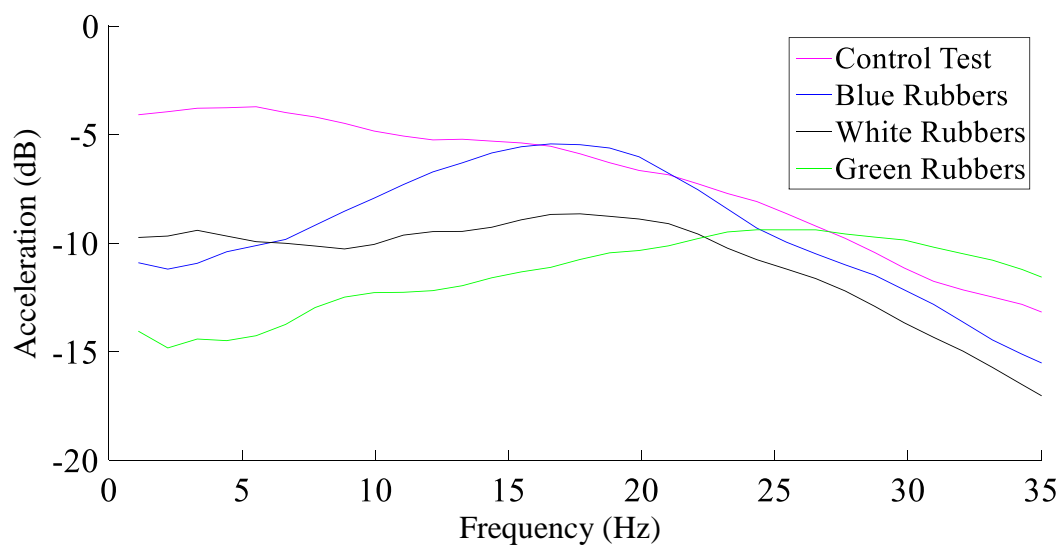


Figure 31: Fast Fourier Transform in the X direction for the MC system.

On the other hand, Figure 32 suggests that Whites are the most appropriate choice in the Y-axis. Greens once again accentuate excitation in the Y-axis, which is consistent with the findings in the Average Maximum Response in the Y-direction. Greens then taper off and follow the Control Test closely. Thus, from the perspective of the Y-axis, it would be better to have no Greens at all, and install Whites.

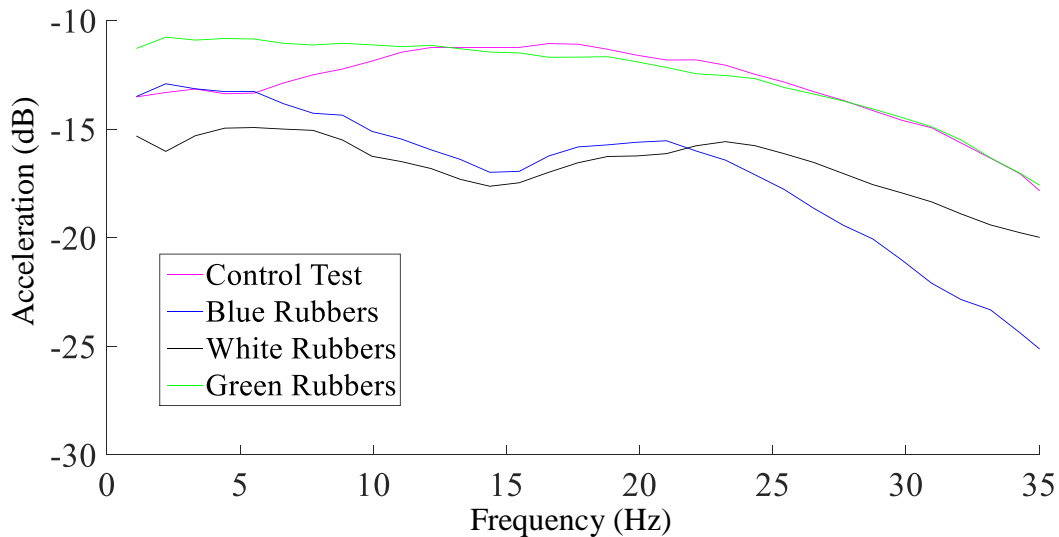


Figure 32: Fast Fourier Transform in the Y-direction for the MC system.

Lastly, in the Z-direction (Figure 33), Blues have the lowest excitation from 0 – 6Hz. However, at slightly larger frequencies, Blues exceed the Control Test response. Greens on the other hand remain relatively consistent from 0 – 10Hz and have a relatively low excitation response. Whites appear quite inactive and do not favour any frequencies in particular, yet for the bandwidth of 0 – 10Hz, it is outperformed by Greens and Blues (for the most part).

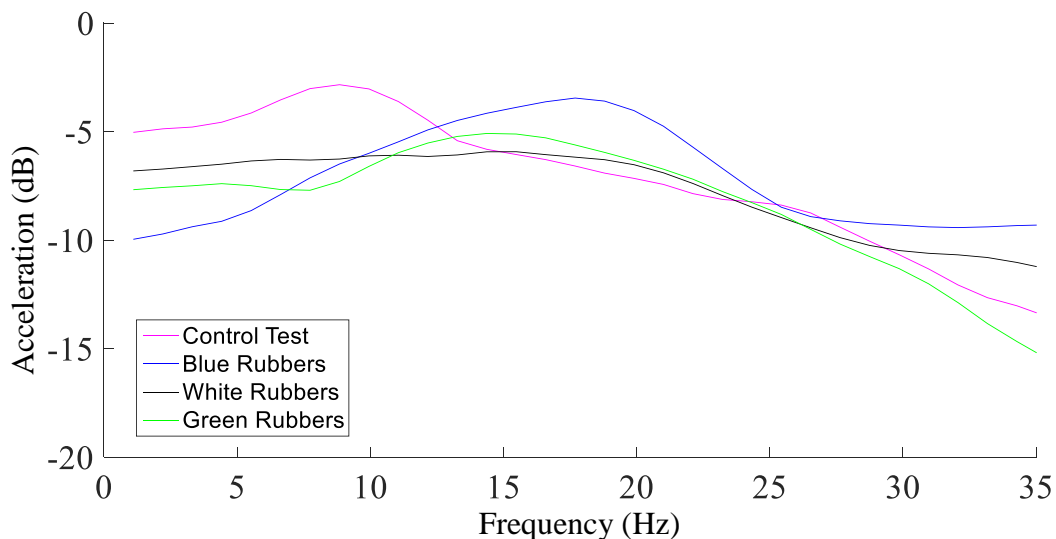


Figure 33: Fast Fourier Transform in the Z direction for the MC system.

Set Selection

Given the weightings of the three axes, Greens perform the best in both the X and Z axes according to the Average Maximum Response and the Fast Fourier Transform for low frequencies. Greens do not perform as well in the Y-axis and render the situation worse. However, given that the Y-axis experiences the least excitation according to the field test, it is a reasonable choice to select the Green set. In addition, this is the only set that can withstand both shear and axial loads with appropriate safety factors (1.83 and 3.49 respectively).

Lighter Component Mass System

Three Axes Average Maximum Response

Figure 34 suggests that all sets perform at roughly the same level (37% – 45% reduction) with Blues having the greatest reduction.

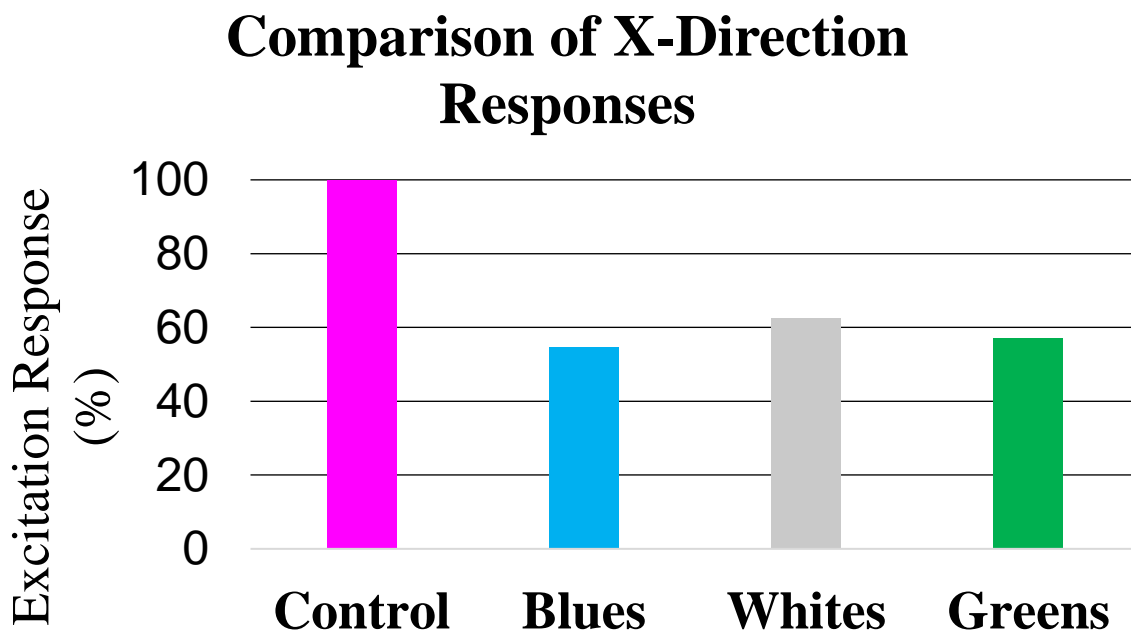


Figure 34: Average Maximum Response in the X-direction for the lighter component system.

Yet in the Y-direction (Figure 35), Blues only reduce by 8% and are outperformed by Greens (29% reduction).

Comparison of Y-Direction Responses

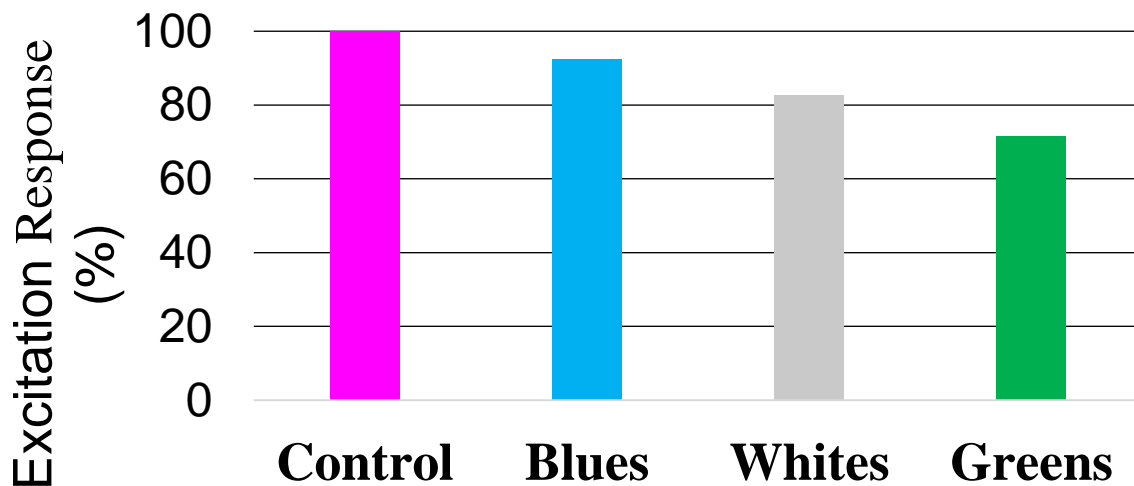


Figure 35: Average Maximum Response in the Y-direction for the lighter component system.

Lastly, in the Z-direction (Figure 36), Blues significantly reduce shock transmission by only responding by half of the excitation. Greens respond the most but still performs well (27% reduction).

Comparison of Z-Direction Responses

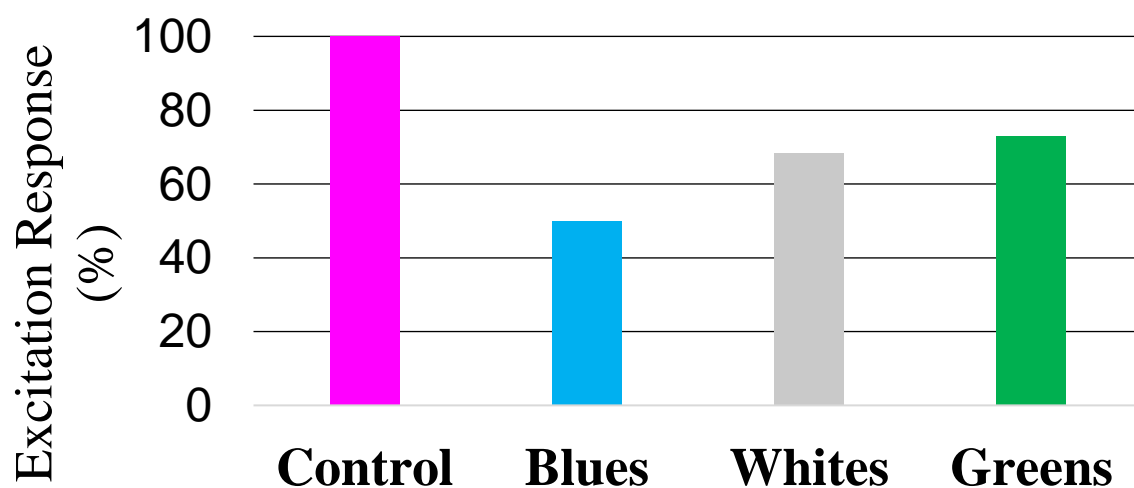


Figure 36: Average Maximum Response in the Z-direction for the lighter component system.

Three Axes Fast Fourier Transform

Figure 37 suggests that for low frequencies, the Greens respond the least, followed closely by blue. Both sets remain completely under the Control Test, Whites on the other hand exceed it at about 10 Hz.

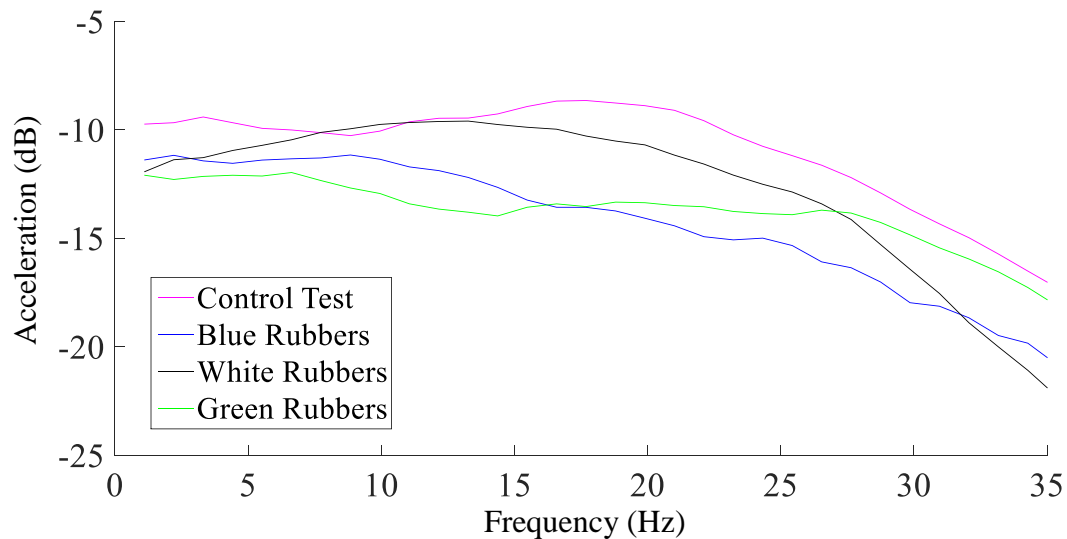


Figure 37: Fast Fourier Transform in the X-direction for the lighter components system.

In the Y-direction (Figure 38), Blues render the excitations worse by having accentuated responses at these lower frequencies. In this case, the Whites would be the most appropriate choice.

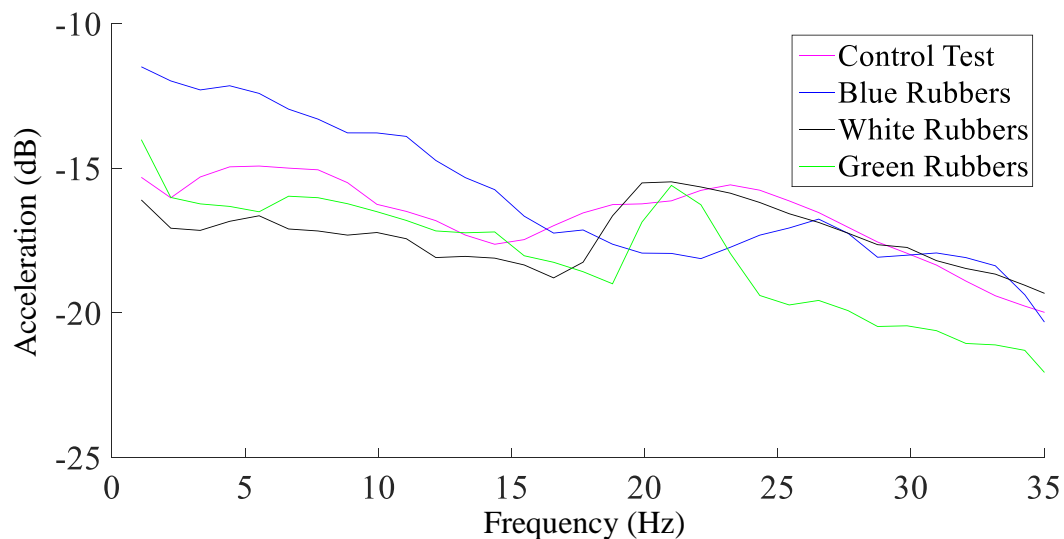


Figure 38: Fast Fourier Transform in the Y-direction for the lighter components system.

Lastly, for the Z-axis (Figure 39), the Blues significantly outperform the other sets. It remains relatively consistent from 0 – 23Hz. Greens, however, have a greater response at the lower frequencies.

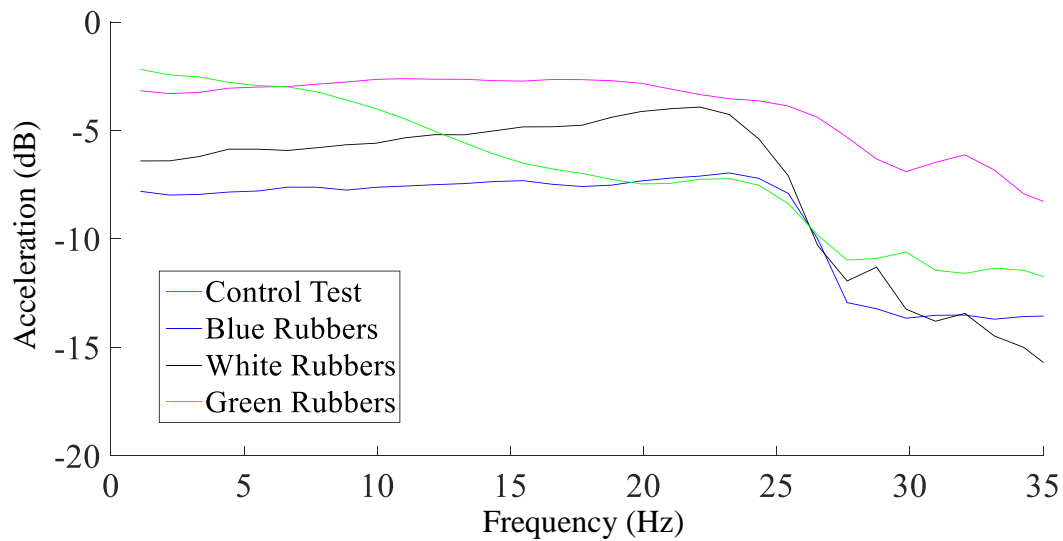


Figure 39: Fast Fourier Transform in the Z-direction for the lighter components system.

Set Selection

Based off the findings from the Average Maximum Response, and the Fast Fourier Transform, the Blues were the most appropriate choice given its superior performance in the X- and Z-axes. Once again, the trend of poor performance in the Y-axis is present.

In terms of loading, it can withstand the axial and shear forces from the field test, with a safety factor of 3.78 and 1.89 respectively. Hence, the Blue set has been selected for the lighter mass system.

Comments on the Y-Axis

Based off the selected rubbers, the Y-axis on the mounting system is the most responsive and accentuates shocks.

Given that the Y-axis in the field test experiences the least excitation, it would be ideal to align the Y-axis of the mounting system to that of the PWC. This means that the most responsive axis is aligned with the one that receives the least excitation.

Installation of Mounting System

Now that the appropriate rubber sets had been identified for the mass systems, the next step was to install the mounting system.

Firstly, the laminated wood had to be removed. This was chiselled out from the PWC, and the remaining surface was sanded smooth, see Figures 40, 41, and 42.

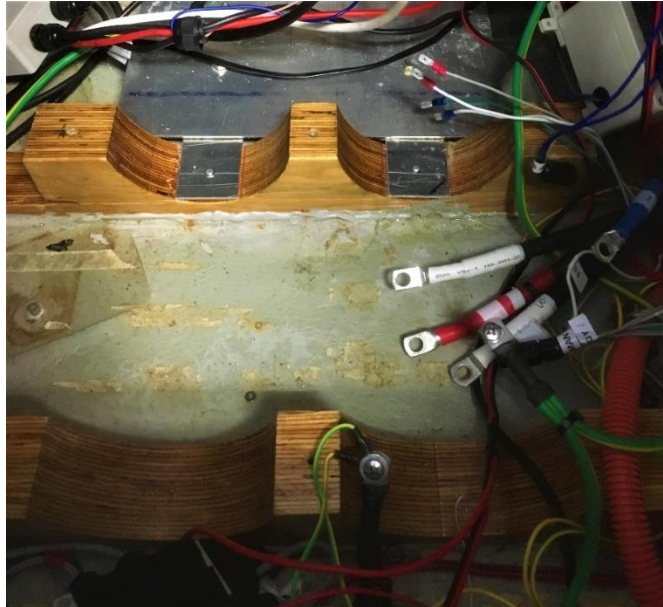


Figure 40: Laminated wooden cradles prior to removal.

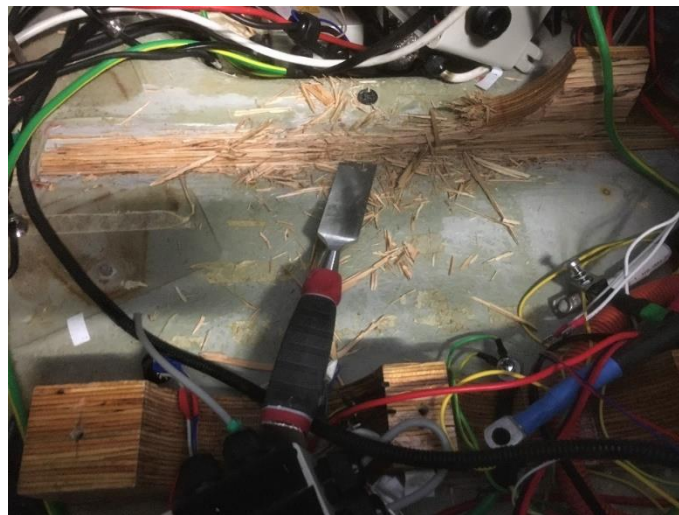


Figure 41: Laminated wooden cradle being chiselled apart.



Figure 42: One laminated wooden cradle removed.

To save on costs, two wooden blocks were salvaged from the testing frame. These were sanded smooth, dusted, and cleaned. All blocks including the new crossbeam were coated and allowed to dry (Figure 44). The crossbeam that once supported the fuse box was created out of laminated wood. This was removed and replicated with structural pine to improve the structural integrity of the mount (Figure 43).



Figure 43: A comparison between the original laminated crossbeam (top), versus the structural pine crossbeam (bottom).



Figure 44: The wooden blocks and new crossbeam were coated to prevent rot.

Having taken down all the necessary dimensions, and made the corresponding markings on the PWC hull, the blocks were adhered to the fiberglass. Heavy objects were placed on top while the adhesive cured to ensure a strong bond, see Figures 45, 46, and 47.



Figure 45: The underside of a block was covered in glue (left), about to be placed on the fiberglass (right).



Figure 46: The block was in place, heavy objects were placed on top to allow for a strong bond to develop while the glue cures.



Figure 47: The blocks were now adhered to the hull.

Once the new crossbeam was installed (Figure 48), it was followed by the rubber mounts (Figure 49) and the plate (Figure 50).



Figure 48: The crossbeam was installed (top).



Figure 49: The Green rubber mounts were installed (corners).

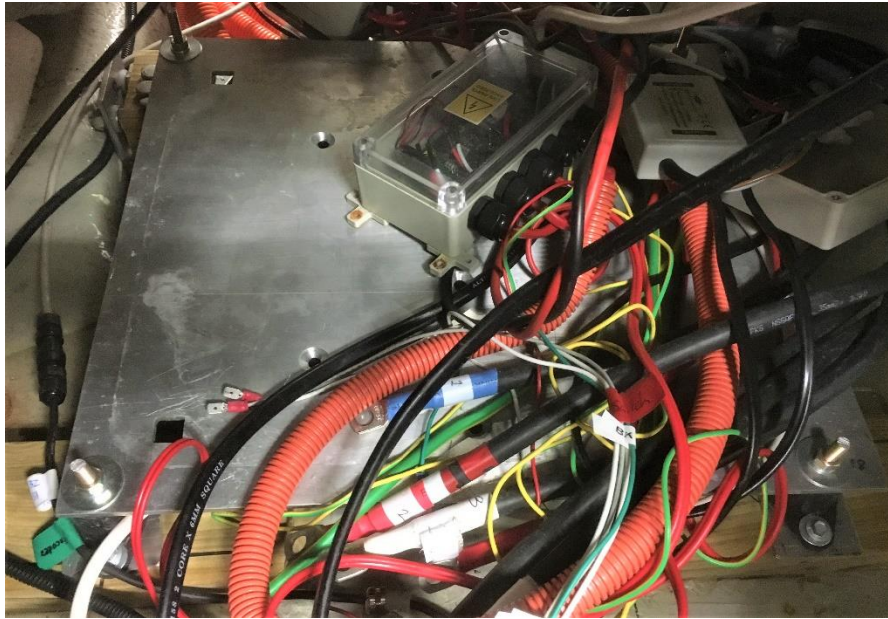


Figure 50: The MC plate was fastened to the rubber mounts. The presence of spring washers are most evident under the nut in the top left corner (one per nut). This prevents the nuts from coming loose due to vibrations.

The MC box was installed (Figure 51 and 52) and bolted down to its plate. The Y-axis of the mount during its test, and that of the PWC are aligned. Thus, minimizing excitations in the Y-axis.

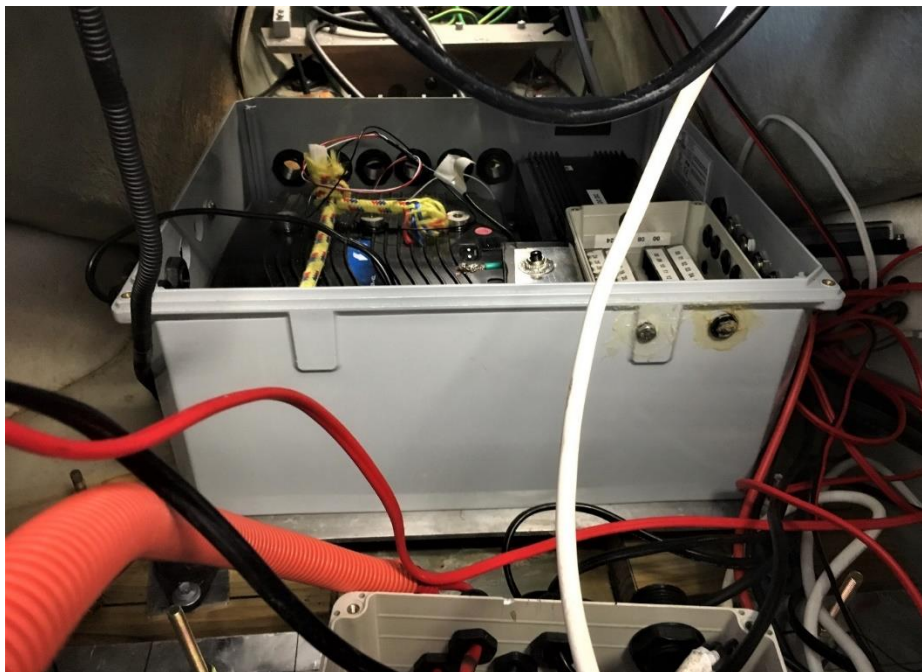


Figure 51: The MC box was installed onto the plate and fastened.

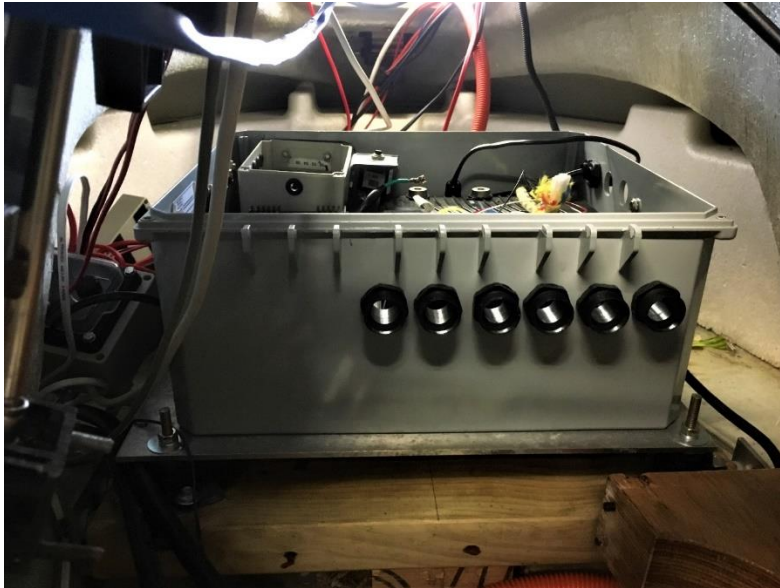


Figure 52: The MC box installed, view from the rear.

The same process was undertaken for the lighter components. Adhesive Velcro strips were placed onto the fuse box plate and on all the smaller components as well. These were then mounted, see Figure 53 and 54.

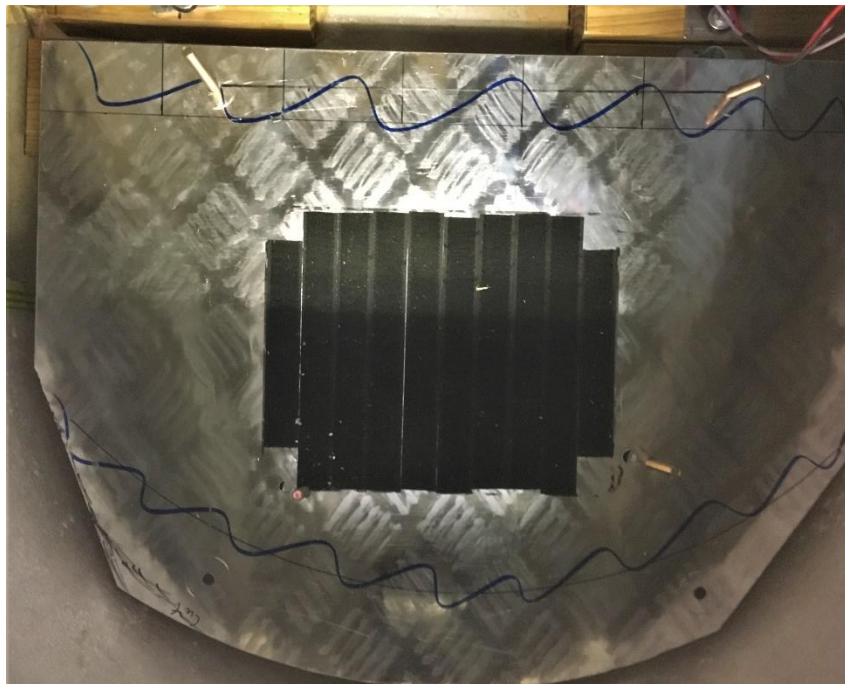


Figure 53: The fuse box plate was placed in the bow of the PWC, on top of the Blue set.



Figure 54: Smaller components being mounted onto the plate with Velcro strips.

However, the drawback of this design for the smaller components was that the Y-axis cannot align due to the shape of the plate. This implies that the X-axis excitations from the PWC are received by the Y-axis of the mount. And, based off the choice of Blues, this accentuates the shocks and vibrations. Although this may be the case, it is worth noting that the extent of excitation in the X-axis for the PWC is still relatively small when compared to the Z-axis. Thus, the benefits of this system outweigh the disadvantages. It is worth acknowledging that this mount has two additional benefits, outlined in **Appendix 3**.

Conclusion

To summarize, the electric PWC has several electrical components that require protection from shocks and vibrations caused by waves on the water, and from road features. Of all the axis that require the greatest shock absorption, it is the vertical axis. Various vibration isolation methods were considered but ultimately the most appropriate choice was the rubber mounts.

Three sets of rubber mounts were purchased due to budget constraints and were tested in the laboratory by constructing a testing frame. The data collected was then processed and analysed to produce an Average Maximum Response and Fast Fourier Transform. From these two outcomes, the most appropriate set for the MC box was determined to be the Greens, and likewise the Blues for the lighter components such as the fuse box. The PWC is now equipped with the appropriate isolators to protect its electrical components.

Future Work

In terms of vibration and shock isolation, future students may wish to explore the benefits of harder rubbers for the MC system. The fuse box plate cannot employ a softer rubber mount from Embelton as it does not exist. However, whilst the Greens are sufficient, other sets such as Yellows and the NR2 set from the specification sheet remain untried. This alone, however, would not be sufficient for a thesis and would not be solving a significant problem, only optimizing an existing system.

Mechanical engineering students who are interested in vibration and shock isolation could consider a research thesis on active isolation. It would be best to assess its suitability for the PWC. Considerations would include the power draw, number of additional components, the reduction in ride time, and cost to name a few.

Other aspects outside the scope of this project would be to develop a new charging system for individual tubes. There are eight cells in parallel for one section (Figure 55). In the three large tubes there are eight sections, and for the two smaller tubes there are three sections. Very often, certain cells die because the voltage is below its threshold, or it is overcharged. Hence to prevent this, the cells have to be rebalanced. This process of balancing cells is extremely time consuming and often hinders the students from conducting their field tests. It also means that students must spend more time working on fixing or maintaining the PWC instead of focusing on their research project.



Figure 55: The cells within a large tube, with each section consisting of eight parallel cells.

Currently, the cells are balanced through a voltmeter box (Figure 56). However, due to fuses within the tubes the amperage cannot exceed 2amps, this is extremely time consuming.

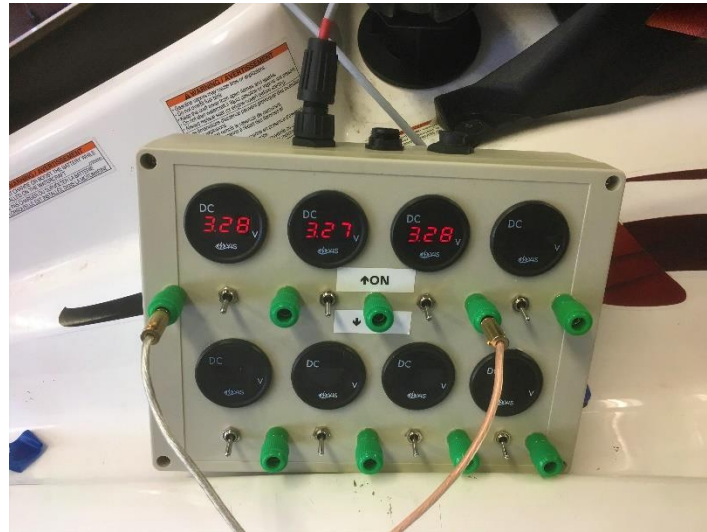


Figure 56: Charging/balancing cells through the voltmeter box.

The alternative was to extract the cells from the tube and bypass the fuses by charging directly. This is an inconvenience and also means that the tubes must be disconnected from each other and extracted. Hence, a means to charge individual sections quickly without extracting the cells from the tube or blowing the fuses within the tube is greatly sought after. Of course, there must also be a means of monitoring the voltage during the charge as well.

References

- Accurion 2018, *Principles of Halcyonics Active Vibration Isolation Technology*. Available from: <https://www.accurion.com/active-vibration-isolation-technology>. [9 December 2017].
- Adafruit n.d., *Code Walkthrough*. Available from: <https://learn.adafruit.com/adafruit-data-logger-shield/using-the-real-time-clock-3>. [11 March 2018].
- Analog Devices 2009, *Digital Accelerometer ADXL345*. Available from: www.analog.com. [23 February 2018].
- Arduino 2018, *What is Arduino?*. Available from: <https://www.arduino.cc/en/Guide/Introduction>. [19 February 2018].
- Audio-Technica 2018, *How do active noise-cancelling headphones work?*. Available from: <https://www.audio-technica.com/cms/features/b3ef06fca462fcad/>. [14 December 2017].
- Chains & Drives 2018, *Vibration Mounts*. Available from: <https://www.chainanddrives.com.au/products/vibration-mounts>. [13 April 2018].
- Chau, L 2017, *Modelling and Design of Mounting System for an Electric Personal Watercraft*, MPE, thesis University of Western Australia.
- ClimateNexus 2018, *Animal Agriculture's Impact on Climate Change*. Available from: <https://climatenexus.org/climate-issues/food/animal-agricultures-impact-on-climate-change/>. [22 April 2018].
- Curtis Instruments 2009, *Manual AC Induction MCs*, CI, New York.
- Embelton 2011, *Rubber Mounts Type NR/NRD*. Available from: <http://vibration-isolation.embelton.com/anti-vibration-mounts/rubber-mounts/>. [14 April 2018].
- Friedrich, C 1998, *Transmissibility Chart*, image. Available from: <http://pages.mtu.edu/~microweb/chap2/ch2-8.htm>. [25 March 2018].
- Github, Inc. 2018, *SparkFun ADXL345 Arduino Library*. Available from: https://github.com/sparkfun/SparkFun_ADXL345_Arduino_Library. [2 March 2018].
- Harris, C 2002, *Harris' Shock and Vibration Handbook*, McGraw-Hill, USA. Available from: Book Depository. [24 March 2018].
- Heckbert, P 1995, 'Fourier Transforms and the Fast Fourier Transform (FFT) Algorithm', *Semanticscholar*, pp.4.
- Hunt, E 2017, 'Most Australians want renewables to be primary energy source , survey finds', *The Guardian*, 27 June. Available from: <https://www.theguardian.com/australia-news/2017/jun/27/most-australians-want-renewables-to-be-primary-energy-source-survey-finds>. [22 April 2018].
- Jensen, C 2015, *Design and Installation of Mounting Systems for an Electric Personal Watercraft*, MPE, thesis University of Western Australia.

Jones, N 2017, 'How the World Passed a Carbon Threshold and Why It Matters', *Yale Environment 360*. Available from: <https://e360.yale.edu/features/how-the-world-passed-a-carbon-threshold-400ppm-and-why-it-matters>. [22 April 2018].

Knight, R 2014, 'The Oxidation of Aluminium', *Corrosion Pro Articles*. Available from: <http://www.corrosionpro.com/blog/the-oxidation-of-aluminum/>. [5 January 2018].

LearnThermo n.d., *Conversion of Kinetic Energy into Spring Potential Energy*. Available from: <https://www.learnthermo.com/examples/ch01/p-1a-2.php>. [1 April 2018].

Liu, Y 2017, Redesign of REV Ski stability and handling, MPE, thesis University of Western Australia.

MIT OpenCourseWare 2013, *2.1 Vibration Isolation*, YouTube video, 3 September. Available from: <https://www.youtube.com/watch?v=f1pxiNDTyHc>. [25 March 2018].

Mohamed, A 2015, *Simple and Easy Tutorial on FFT Fast Fourier Transform Matlab Part 1*, YouTube video, 22 November. Available from: <https://www.youtube.com/watch?v=3FAIXEkxyBs&t=611s>. [10 April 2018].

National Instruments 2017, *Measuring Vibrations with Accelerometers*. Available from: <http://www.ni.com/white-paper/3807/en/>. [4 December 2017].

Polymer Technologies 2014, *Passive and Active Isolation Systems... What's the Difference?*. Available from: <http://blog.polytechinc.com/passive-and-active-isolation-systems...whats-the-difference>. [9 December 2017].

Quora 2016, *What is the role of viscosity in shock absorbers?*. Available from: <https://www.quora.com/What-is-the-role-of-viscosity-in-shock-absorbers>. [14 March 2018].

Redmon, N 2002, *A gentle introduction to FFT*. Available from: <http://www.earlevel.com/main/2002/08/31/a-gentle-introduction-to-the-fft/>. [7 April 2018].

Rouse, M 2005, *Nyquist Theorem*. Available from: <https://whatis.techtarget.com/definition/Nyquist-Theorem>. [4 December 2017].

Shock Absorber n.d., image. Available from: https://en.wikipedia.org/wiki/Shock_absorber. [14 March 2018].

Total Materia 2002, *Corrosion of Zinc*. Available from: <http://www.totalmateria.com/Article40.htm>. [5 January 2018].

Vibration Damage 2018, *Vibration Frequency*. Available from: http://vibrationdamage.com/vibration_frequencies.htm. [18 March 2018].

Wenzel Metal Spinning n.d., *Galvanized vs Stainless Steel*. Available from: <https://www.wenzelmetalspinning.com/galvanized-steel-vs-stainless.html>. [5 January 2018].

Williams, M 2015, *What is Hooke's Law?*. Available from: <https://phys.org/news/2015-02-law.html>. [18 March 2018].

Appendices

Appendix 1: Arduino Uno Accelerometer Code

```
#include <SPI.h>

#include <SD.h>

#include <SparkFun_ADXL345.h>    // SparkFun ADXL345 Library
ADXL345 adxl = ADXL345();      // USE FOR I2C COMMUNICATION

const int chipSelect = 4;

File dataFile;

void setup() {

  Serial.begin(9600);          // Start the serial terminal
  Serial.println("SparkFun ADXL345 Accelerometer Hook Up Guide Example");
  Serial.println();

  adxl.powerOn();             // Power on the ADXL345

  adxl.setRangeSetting(4);     // Set the accelerometer threshold.
  // Accepted values are 2g, 4g, 8g or 16g
  // Higher Values = Wider Measurement Range
  // Lower Values = Greater Sensitivity

  adxl.setActivityXYZ(1, 0, 0); // Set to activate movement detection in the axes
  "adxl.setActivityXYZ(X, Y, Z);" (1 == ON, 0 == OFF)

  adxl.setActivityThreshold(75); // 62.5mg per increment // Set activity // Inactivity
  thresholds (0-255)

  adxl.setInactivityXYZ(1, 0, 0); // Set to detect inactivity in all the axes
  "adxl.setInactivityXYZ(X, Y, Z);" (1 == ON, 0 == OFF)
```

```
adxl.setInactivityThreshold(75); // 62.5mg per increment // Set inactivity // Inactivity thresholds (0-255)
```

```
adxl.setTimeInactivity(10); // How many seconds of no activity is inactive?
```

```
adxl.setTapDetectionOnXYZ(0, 0, 1); // Detect taps in the directions turned ON  
"adxl.setTapDetectionOnX(X, Y, Z);" (1 == ON, 0 == OFF)
```

```
// Set values for what is considered a TAP and what is a DOUBLE TAP (0-255)
```

```
adxl.setTapThreshold(50); // 62.5 mg per increment
```

```
adxl.setTapDuration(15); // 625  $\mu$ s per increment
```

```
adxl.setDoubleTapLatency(80); // 1.25 ms per increment
```

```
adxl.setDoubleTapWindow(200); // 1.25 ms per increment
```

```
// Set values for what is considered FREE FALL (0-255)
```

```
adxl.setFreeFallThreshold(7); // (5 - 9) recommended - 62.5mg per increment
```

```
adxl.setFreeFallDuration(30); // (20 - 70) recommended - 5ms per increment
```

```
// Setting all interrupts to take place on INT1 pin
```

```
//adxl.setImportantInterruptMapping(1, 1, 1, 1, 1); // Sets  
"adxl.setEveryInterruptMapping(single tap, double tap, free fall, activity, inactivity);"
```

```
// Accepts only 1 or 2 values for pins INT1 and INT2. This chooses the pin on the  
ADXL345 to use for Interrupts.
```

```
// This library may have a problem using INT2 pin. Default to INT1 pin.
```

```
// Turn on Interrupts for each mode (1 == ON, 0 == OFF)
```

```
adxl.InactivityINT(1);
```

```
adxl.ActivityINT(1);
```

```
adxl.FreeFallINT(1);
```

```
adxl.doubleTapINT(1);
```

```
adxl.singleTapINT(1);
```

```

//attachInterrupt(digitalPinToInterrupt(interruptPin), ADXL_ISR, RISING); // Attach
Interrupt
Serial.print("Initializing SD card...");

// make sure that the default chip select pin is set to
// output, even if you don't use it:
pinMode(SS, OUTPUT);

// see if the card is present and can be initialized:
if (!SD.begin(chipSelect)) {
  Serial.println("Card failed, or not present");
  // don't do anything more:
  while (1) ;
}
Serial.println("card initialized.");

// Open up the file we're going to log to!
dataFile = SD.open("datalog.csv", FILE_WRITE);
if (! dataFile) {
  Serial.println("error opening datalog.csv");
  // Wait forever since we cant write data
  while (1) ;
}
}

/***** MAIN CODE *****/

/* Accelerometer Readings and Interrupt */
void loop() {

// Accelerometer Readings

```

```
int x, y, z;

adxl.readAccel(&x, &y, &z);    // Read the accelerometer values and store them in
variables declared above x,y,z

// Output Results to Serial
/* UNCOMMENT TO VIEW X Y Z ACCELEROMETER VALUES */
Serial.print(x);
Serial.print(" ");
Serial.print(y);
Serial.print(" ");
Serial.println(z);
dataFile.print(x);
dataFile.print(" ");
dataFile.print(y);
dataFile.print(" ");
dataFile.println(z);
dataFile.flush();
delay(250);    // Set the delay to a quarter of a second.
}
```

Appendix 2: MATLAB Fourier Transform Code

MATLAB Code Usage

This MATLAB code was based off a code by Mohamed (2015), and was further developed for this project.

The Fourier Transform was applied to each test (Control and the three rubber sets). A code was developed for each, the sole difference was the symbol for the average of the combined matrices:

- Mean Control Test Matrix: *MCT*
- Mean Blues: *MB*
- Mean Whites: *MW*
- Mean Greens: *MG*

The MATLAB code was run to obtain the average combined matrix of all the Fourier Transforms conducted on that one test. The average is only obtained after the Fourier Transform had taken place. This yields *MCT* for the Control test, this is then repeated to obtain *MB*, *MW*, and *MG*. All these matrices and the frequency vector, *freq* were saved manually. The Control test code is presented below, for Blues, *MCT* is replaced by *MB*, and so on for the other sets. It is also worth noting that all the input variables are indicating the z axis. This is simply a matter of notation and was still implemented for other axes, another code was not generated solely to keep with notation sake.

Control Test Code

```
Fs = 70.76666; %Sampling Frequency
```

```
Ts = 1/Fs; %Sampling Period
```

```
dt = 0.028261894:Ts:0.989166274-Ts; %Signal Duration
```

```
nfft = (0.989166274-0.028261894)*Fs; %Length of time domain signal
```

```
nfft2 = 2.^nextpow2(nfft); %Length represented as a power of 2
```

```
ff1 = fft(z1, nfft2); %Fast Fourier Transforms for each trial
```

```
ff2 = fft(z2, nfft2);
```

```
ff3 = fft(z3, nfft2);
```

```
ff4 = fft(z4, nfft2);
```

```
ff5 = fft(z5, nfft2);
```

```
ff6 = fft(z6, nfft2);
```

```
ff7 = fft(z7, nfft2);
```

```
ff8 = fft(z8, nfft2);
```

```

ff9 = fft(z9, nfft2);
ff10 = fft(z10, nfft2);

n = length(ff1); %Number of terms in the FFT matrices
freq =(1:n/2)/(n/2)*Fs; %The span of frequencies

```

```

%Removing the dual

```

```

A1 = abs(ff1/length(ff1));
B1 = A1(1:length(ff1)/2+1,:);
B1(2:end-1,:) = 2*B1(2:end-1,:);
ff1 = B1;
ff1(1)=[];

```

```

A2 = abs(ff2/length(ff2));
B2 = A2(1:length(ff2)/2+1,:);
B2(2:end-1,:) = 2*B2(2:end-1,:);
ff2 = B2;
ff2(1)=[];

```

```

A3 = abs(ff3/length(ff3));
B3 = A3(1:length(ff3)/2+1,:);
B3(2:end-1,:) = 2*B3(2:end-1,:);
ff3 = B3;
ff3(1)=[];

```

```

A4 = abs(ff4/length(ff4));
B4 = A4(1:length(ff4)/2+1,:);
B4(2:end-1,:) = 2*B4(2:end-1,:);
ff4 = B4;

```

```
ff4(1)=[];
```

```
A5 = abs(ff5/length(ff5));
```

```
B5 = A5(1:length(ff5)/2+1,:);
```

```
B5(2:end-1,:) = 2*B5(2:end-1,:);
```

```
ff5 = B5;
```

```
ff5(1)=[];
```

```
A6 = abs(ff6/length(ff6));
```

```
B6 = A6(1:length(ff6)/2+1,:);
```

```
B6(2:end-1,:) = 2*B6(2:end-1,:);
```

```
ff6 = B6;
```

```
ff6(1)=[];
```

```
A7 = abs(ff7/length(ff7));
```

```
B7 = A7(1:length(ff7)/2+1,:);
```

```
B7(2:end-1,:) = 2*B7(2:end-1,:);
```

```
ff7 = B7;
```

```
ff7(1)=[];
```

```
A8 = abs(ff8/length(ff8));
```

```
B8 = A8(1:length(ff8)/2+1,:);
```

```
B8(2:end-1,:) = 2*B8(2:end-1,:);
```

```
ff8 = B8;
```

```
ff8(1)=[];
```

```
A9 = abs(ff9/length(ff9));
```

```
B9 = A9(1:length(ff9)/2+1,:);
```

```
B9(2:end-1,:) = 2*B9(2:end-1,:);
```

```
ff9 = B9;
```

```
ff9(1)=[];
```

```
A10 = abs(ff10/length(ff10));
```

```
B10 = A10(1:length(ff10)/2+1,:);
```

```
B10(2:end-1,:) = 2*B10(2:end-1,:);
```

```
ff10 = B10;
```

```
ff10(1)=[];
```

```
All = cat(2, ff1, ff2, ff3, ff4, ff5, ff6, ff7, ff8, ff9, ff10); %Combination of all FFT matrices
```

```
MCT = mean(All, 2); %Average of the combined matrices
```

```
%Generation of plots
```

```
subplot(6,2,1)
```

```
plot(freq,abs(ff1))
```

```
subplot(6,2,2)
```

```
plot(freq,abs(ff2))
```

```
subplot(6,2,3)
```

```
plot(freq,abs(ff3))
```

```
subplot(6,2,4)
```

```
plot(freq,abs(ff4))
```

```
subplot(6,2,5)
```

```
plot(freq,abs(ff5))
```

```
subplot(6,2,6)
```

```
plot(freq,abs(ff6))
```

```
subplot(6,2,7)
```

```
plot(freq,abs(ff7))
```

```
subplot(6,2,8)
```

```
plot(freq,abs(ff8))
```

```

subplot(6,2,9)
plot(freq,abs(ff9))
subplot(6,2,10)
plot(freq,abs(ff10))
subplot(6,2,11)
plot(freq,abs(MCT)) %Plot the MCT matrix against the frequency vector

```

Plotting the Results

With all the average matrices and frequency vector saved, the following code may be implemented to plot the average Fourier Transform. The generated plot represents each test for the axis in question and the relevant mass system.

Plot Generation Code

```

close all %Close all figures.
hold on %Allow more than one curve on the plot.
plot(freq,20*log10(MCT),'m') %Plot MCT and freq in magenta.
plot(freq,20*log10(MB),'b') %Plot MB and freq in blue.
plot(freq,20*log10(MW),'k') %Plot MW and freq in black.
plot(freq,20*log10(MG),'g') %Plot MG and freq in green.
legend('Control Test','Blue Rubbers','White Rubbers','Green Rubbers')
xlim([0 35]) %limits the display of the X axis to only 35Hz as per the Nyquist Theorem.
set(gca,'fontsize',15) %Set the font to size 15.

```

Appendix 3: Additional Benefits

This mounting system has brought about two additional benefits.

Tube Loading

The MC mount was designed to allow for sufficient clearance above the box to avoid collisions or blockage with the top of the PWC, and place additional components (Figure 57). However, given that there was sufficient clearance, battery tubes may now be loaded in through the front (Figure 58 and 59). This significantly facilitates the assembly process and loading tubes from the rear is a challenge and can be damaging to the cables.



Figure 57: Sufficient clearance for a battery tube.



Figure 58: Starting to load a battery tube through the front.

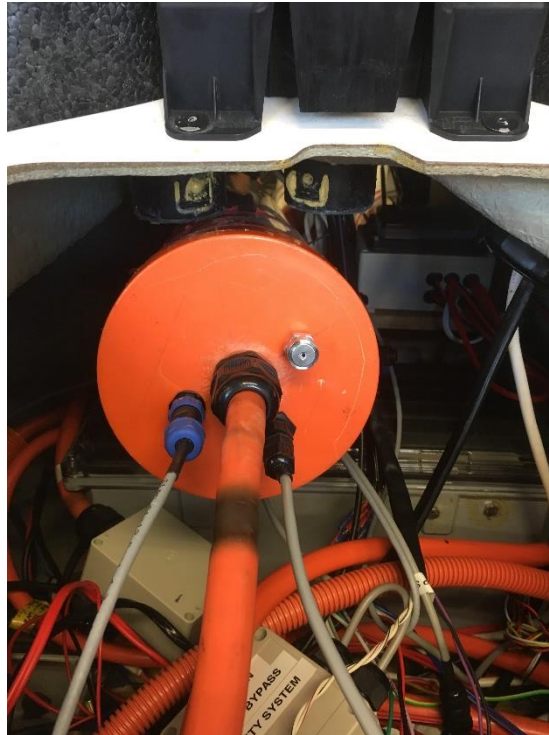


Figure 59: Inserting a battery tube deeper, from the front.

Centre of Mass

Without undergoing an extensive explanation, the MC box was placed closer to the bow prior to the start of this project. Now that it has been relocated further from the box, and towards the rear (~40cm), the centre of mass of the entire PWC has been shifted further to the rear. This would in turn lift the nose of the PWC further out of the water and as a result improve the ride performance.

Appendix 4: Additional Research

Sampling Frequency

A common method to measure vibrations is with an accelerometer (National Instruments 2017). According to the Nyquist Theorem, the sampling frequency of the accelerometer must be at least twice of the excitation frequency, else the higher frequencies will not be measured accurately as it is beyond the bandwidth of the accelerometer (Rouse 2005).

Fourier Transform

From Fourier's research on periodic waveforms, it is now known that these may be represented as a summation of sine waves. The Fourier Transform deconstructs the periodic waveforms into these individual sine waves. This is known as forward Fourier Transform, where the waves are transferred from the time domain into the frequency domain (Redmon 2002). This determines all the frequencies present in the wave (Vibration Damage 2018).

The Fourier Transform was initially continuous but may be discretised to compute the Discrete Fourier Transform, allowing it for applications in non-analytical situations. The Fast Fourier Transform is simply a fast algorithm that computes the Discrete Fourier Transform, by reducing the complexity of operations (Heckbert 1995).